The University of Hawai‘i at Mānoa

The Design and Simulated Performance of the Attitude Determination and Control System of a Gravity Gradient Stabilized Cube Satellite

Windell Harold Jones

A master’s project report submitted to the mechanical engineering department of the University of Hawai‘i at Mānoa in partial fulfillment of the requirements for the degree of Master of Science in Mechanical Engineering

May 2014

Exam Committee:

Brian Bingham, Chairperson
Wayne Shiroma
Reza Ghorbani

This is dedicated first to my beloved wife Maryam and my son Isaiah. Your love is forever unfailing. Second, this is to all those engineering students who walked instinctually step by step through their studies, taking too long to graduate, and not sure where their decisions would lead them. Then little did you know that when you looked back, you realized that what seemed to be a chaotic journey was actually an elegant path of unintended order.

“Everything should be made as simple as possible, but not simpler.”

—Albert Einstein

“Failure is an option here. If things are not failing, you are not innovating enough.”

—Elon Musk

Acknowledgements

I would like to begin by first thanking my thesis advisor, Dr. Brian Bingham, for always supporting me with my graduate work. He has always had a strong eye to keep me on track by maintaining practicality while still appreciating the theoretical and complex concepts of spacecraft attitude determination and control. He has a good balance between application and theory, and I am fortunate to have him as my advisor.

I would like to express thanks to my supporting committee members Dr. Wayne Shiroma and Dr. Reza Ghorbani for being patient with me during the process of developing this report.

I would like to thank the entire H2 satellite team and the UH Mānoa College of Engineering's Small-Satellite Program for allowing me to be a part of such a momentous event for the University of Hawai'i. All of you are talented individuals; we represent the UH College of Engineering well, and it has been a privilege to work with each of you. Specifically, thank you to Nick Fisher for maintaining a high-level perspective and helping me define the eventual goals I needed to reach during the design of the NADDS that helped determine the impact that H2's ADCS had on H2's mission. Thank you, Larry Martin, for handling all the programmatic duties and boring documentation. We could not have built H2 without you. My late night conversations with you are cherished. Both you and Nick have a gift of getting the ball moving when it gets tough. Thank you to Vincent So and Jon Dang for the late-night coding of much of the ADCS algorithm into H2, and for dealing with my quirkiness. Lastly, thank you, Toy Lim, for your constant dedication to the team, pursuit of teaching, in-depth knowledge of the hardware that was essential for troubleshooting, and for adapting my test bed deployment code to the satellite hardware. It worked flawlessly every time.

Thank you to Dr. George Wilkens and Dr. Nikolaj Nordkvist for helping me with the theoretical aspects of attitude control over the past few years. I am grateful for your patient explanations and willingness to help me in an impromptu fashion whenever I showed up at your door unexpectedly.

Most importantly, to my son Isaiah and my wife Maryam, thank you so much for your unwavering support. Both of you pushed me through the tough times and long nights during the developmental phases of H2's ADCS. Thank you especially to you Maryam, for those long days when you took care of Isaiah while I was working franticly to finish this report on time. I know that at times my progress was unpredictable and my lack of progress was frustrating. Your patience and understanding is limitless. I definitely would not have been able to accomplish this goal without you and I am forever in debt to both of you. I love you both very much!

Abstract

A 3U cube satellite (CubeSat) named Ho‘oponopono (H2) was developed at the UH Mānoa College of Engineering’s Small-Satellite Laboratory. Its mission was to aid in the radar calibration process of U.S. Air Force radar stations by providing a calibration source in orbit. A gravity-gradient Attitude Determination Control System (ADCS) was designed to point H2 in the nadir direction for the entirety of its mission lifetime of one year. The equilibria for gravity-gradient capture of a non-symmetric satellite is derived to give the reader insight into the unique issues associated with achieving gravity-gradient stabilization. To ensure that the functionality and performance requirements were satisfied, the Nanosatellite Attitude Dynamics & Determination Simulator (NADDS) was developed to identify the time and energies required for each mode of the ADCS. It is discovered that a minimum energy of 2.37 kJ would be required to allow H2 to accomplish all of its control modes, but an energy of 14.162 kJ would more realistically be required depending on when the deploy command was sent to H2. These energies correspond to a minimum time of 4.27 hours and a likely time of 14.42 hours. A simple attitude determination scheme called the TRIaxial Attitude Determination (TRIAD) method was simulated, and the nadir error estimate error is investigated. The error was found to be bounded and less than 25 degrees with a 65% probability for the error to be less than 10 degrees.

Table of Contents

List of Tables

List of Figures

Chapter 1
Introduction

1.1 The Rise of the Cube Satellite

The high cost of launching satellites makes it cost prohibitive for universities to conduct research in space using large-scale satellites. Introduced by Stanford professor Bob Twiggs, the cube satellite was presented to circumvent this problem by standardizing a satellite form factor that could fit in the palm of your hand. Figure 1 shows a cube satellite (CubeSat) developed at the California Polytechnic Institute in San Luis Obispo, California. With a 1U CubeSat's mass at only 1.33 kg, this standard would allow more universities to develop their own satellites at a lesser cost by allowing them to be flown as secondary payloads on larger-budget missions. Larger 3U CubeSats could perform considerably complex missions at a fraction of the cost of their larger counterparts. During the past decade, popularity of CubeSat launches have increased due to the high demand of proposed CubeSat missions by universities.

Figure 1: A 1U CubeSat, CP6, developed by Cal Poly SLO [1].

1.2 The RadCal Satellite

Air Force radar stations are used for trajectory tracking of spacecraft, space debris, and asteroids. Tracking provided by these stations are essential to estimating the object's Two-Line Elements (TLEs). Particularly for orbit propagation of asteroid trajectories, a minimal and known tracking error is essential. A satellite orbiting Earth is an ideal reference object to track since it has a highly deterministic path and the orbit path is entirely passive.

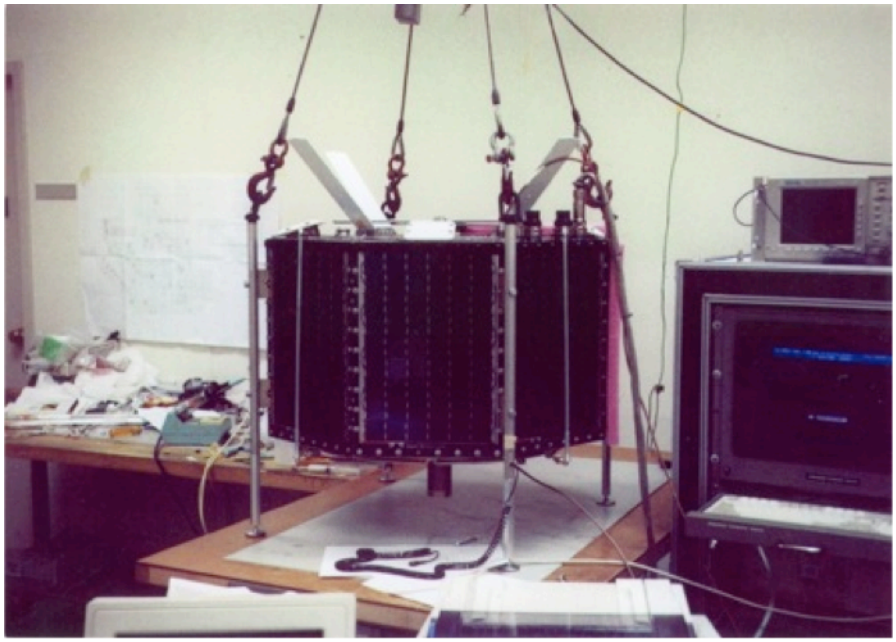

Figure 2: The RadCal satellite undergoing tests prior to launch [3].

Launched on June 25, 1993, RadCal was the first satellite designed solely for calibration of Space Command radar stations (Fig. 2). It was the first satellite dedicated to radar performance monitoring and was also the first satellite to demonstrate attitude determination using GPS. RadCal had a mass of about 90 kg, measured 40.6 cm tall with a diameter of 76.2 cm, and was put into a polar orbit at an altitude of 815 km [2]. It was axially symmetric and passively stabilized using a six-meter gravity-gradient boom. On board, there were two C-band transponders, a dual-frequency Doppler beacon, and a tracking, telemetry and control unit. As an experimental payload and backup orbit determination system,

RadCal also had on board two non-military GPS receivers. The last contact with the RadCal satellite was on May 5, 2013, and although it was designed for only a three-year mission life, it operated for nearly 20 years. It is suspected that both of RadCal's battery charging systems had failed causing it to stop functioning [3].

1.3 Ho‘oponopono's Mission: Radar Calibration

Prior to the failure of the RadCal satellite, the University of Hawai‘i at Mānoa College of Engineering's Small-Satellite Program, led by Dr. Wayne Shiroma, proposed that a CubeSat, Ho‘oponopono (H2), also could perform radar calibration similar to RadCal but with a much smaller form factor. Being a 3U CubeSat, H2 weighs only 4 kg and measures 10 cm by 10 cm by 13.4 cm. Rather than using a Doppler beacon, H2 continuously stores its GPS position and transmits the data down to its ground station for processing. Due to H2's small radar cross-section, it is unfeasible to get returns off the spacecraft's body itself. So H2 has a C-band transponder onboard that responds to interrogations from these radar stations. The responses to radar interrogations allow each radar station to estimate the position of H2 while the GPS data represents an independent estimate of the spacecraft's position. The GPS data is downlinked to the satellite's ground station and processed to form an orbit model for H2. This orbit model is then compared to each radar station's set of position estimates for H2 and corrections are suggested for each radar station to characterize and minimize their tracking error. The concept of H2 performing such a mission was proposed as an experimental technology demonstration mission to the University Nanosatellite Program (UNP) in 2009. The team won third place in the competition and was awarded a total of $220,000 for its development over the course of four years. H2 was launched on November 19, 2013, making it the first satellite designed by the University of Hawai‘i to ever launch into space (Fig. 3).

To close the link budget with the radar stations, the transponder's quadrifilar helix antenna had to be pointed in the nadir direction during interrogation. H2 was designed to meet this requirement using its Attitude Determination and Control

System (ADCS). This system is composed of three parts: a custom-designed five-meter deployable gravity-gradient boom, magnetic torque coils, and a set of low-cost sensors for simple attitude determination. To aid in mission planning and energy budgeting, the time and energy required for each of the ADCS modes of operation needs to be estimated. In addition, the steady state error induced by aerodynamic drag and the disturbance torque caused by the deployment must be estimated to evaluate its impact on the mission. To this end, a custom attitude propagation and control simulator was developed called the Nanosatellite Attitude Dynamics and Determination Simulator (NADDS) in an attempt to answer these questions. The NADDS is also used to validate the function of H2's attitude determination algorithm and characterize its error. The development of the NADDS and description of the hardware for H2's ADCS will be discussed in this project report.

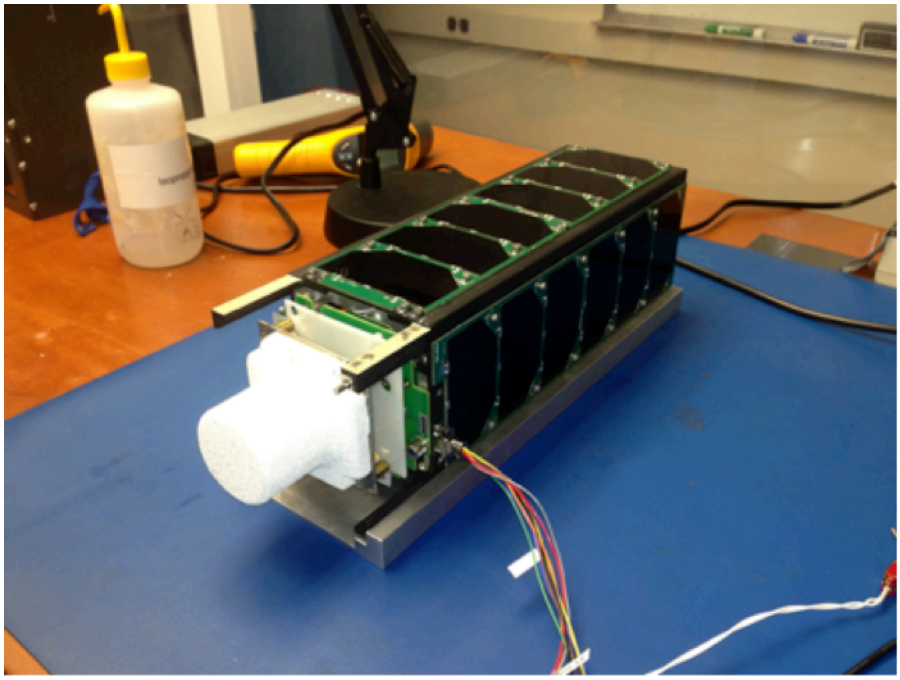

Figure 3: H2 on charge prior to transport for integration into the launch vehicle

Chapter 2

Mathematical Background

The satellite's attitude and angular velocities are always defined in some reference frame. This section begins by describing the different reference frames that are used in NADDS, and how to transform a vector from one frame to another using a rotation matrix. The quaternion is then introduced and how attitude is propagated using the quaternion is described.

2.1 Coordinate Frame Definitions

2.1.1 Earth-Centered Inertial (ECI) Frame

The ECI frame is defined such that its $\hat{\mathrm{I}}$-axis points towards the vernal equinox, $\hat{\mathrm{J}}$-axis points towards along the North Pole or the Earth's rotation axis, and the $\hat{\mathrm{K}}$-axis completes the right-handed coordinate frame (Fig. 4). The ECI frame is not truly inertial since the Earth is accelerating around the Sun on its own orbit. However, the eccentricity of the Earth's orbit, $\epsilon \approx 1.67\times10^{-2}$, is so low that the ECI frame can be considered inertial for our purposes.

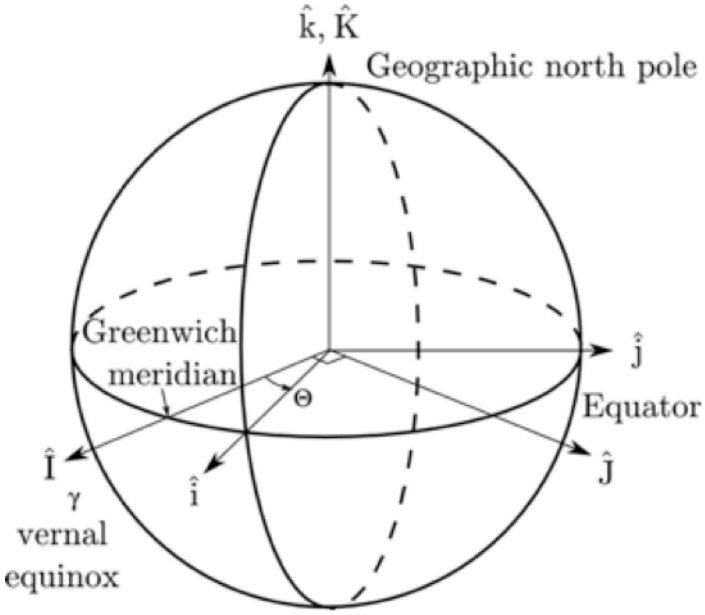

Figure 4: Coordinate frames at Earth's origin

2.1.2 Earth-Centered, Earth-Fixed (ECEF) Frame

Unlike the ECI frame, the ECEF frame rotates with the Earth. Its origin is coincident with the center of the Earth with its $\hat{\mathrm{k}}$-axis along the Earth's rotation axis, $\hat{\imath}$-axis pointing at 0 degrees latitude, and the $\hat{\jmath}$-axis completes the right-handed frame (Fig. 4). The ECEF frame rotates relative to the ECI frame about its $\hat{\imath}$-axis by angle θ.

2.1.3 Local Vertical/Local Horizontal (LVLH) Frame

The LVLH frame has its origin at the center of mass of the spacecraft. Its $\hat{\mathrm{e}}_3$-axis points towards the center of the Earth (nadir direction) and since the spacecraft is assumed to be in a circular orbit, the $\hat{\mathrm{e}}_1$-axis points along the velocity direction of the orbit, and the $\hat{\mathrm{e}}_2$-axis points normal to the orbital plane (Fig. 5).

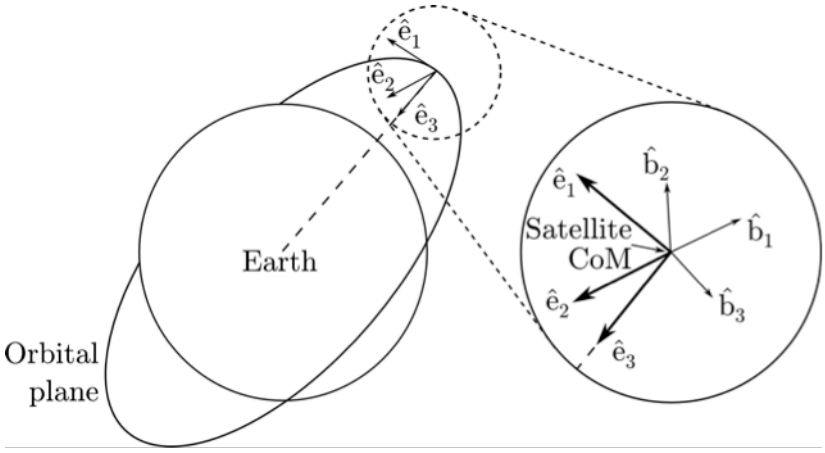

Figure 5: Coordinate frames with origins at satellite's center of mass

2.1.4 Body Frame

The spacecraft body frame has its origin at the center of mass of the spacecraft. The bases of the body coordinate frame are coincident with the principal axes of the spacecraft. The $\hat{\mathrm{b}}_1$-axis is assumed to be the axis of largest inertia, $\hat{\mathrm{b}}_3$ is the minimum inertia axis, and the $\hat{\mathrm{b}}_2$-axis completes the right-handed frame (Fig. 5).

2.2 Attitude Representation and Kinematics

When speaking of the attitude of a spacecraft, this refers specifically to the rotation matrix between a reference coordinate frame and the body frame of the spacecraft. In this case, this is the attitude of the spacecraft body relative to the inertial frame. We begin by first describing the mathematical meaning of the rotation matrix.

2.2.1 The Rotation Matrix

To describe the orientation of the satellite's body with respect to some reference frame such as the inertial frame, the rotation matrix is used to express a vector in one frame in terms of the basis vectors in another. Following the development in [4], assuming the existence of a vector, $\mathbf{v}$, this vector can be described in two different coordinate frames spanned by orthogonal unit vector sets $\{\mathbf{a}_1, \mathbf{a}_2, \mathbf{a}_3\}$ and $\{\mathbf{b}_1, \mathbf{b}_2, \mathbf{b}_3\}$ we can use the following notation:

$$\mathbf{v} = \sum_{i=1}^{3} v_i^a \, \mathbf{a}_i = \sum_{i=1}^{3} v_i^b \, \mathbf{b}_i,$$

where $v_i^a = \mathbf{v} \cdot \mathbf{a}_i$ and $v_i^b = \mathbf{v} \cdot \mathbf{b}_i$ are the coordinates of $\mathbf{v}$ in the frames defined by the basis vector sets $\{\mathbf{a}_1, \mathbf{a}_2, \mathbf{a}_3\}$ and $\{\mathbf{b}_1, \mathbf{b}_2, \mathbf{b}_3\}$ of coordinate frames **A** and **B** respectively. These vectors can be described concisely as

$$\mathbf{v}^a = [v_1^a \; v_2^a \; v_3^a]^T \text{ and } \mathbf{v}^b = \left[v_1^b \; v_2^b \; v_3^b\right]^T.$$

Relating $\mathbf{v}^a$ and $\mathbf{v}^b$ element-wise,

$$\mathbf{v}_i^a = v \cdot \mathbf{a}_i = \left(v_1^b \mathbf{b}_1 + v_2^b \mathbf{b}_1 + v_3^b \mathbf{b}_1\right) \cdot \mathbf{a}_i = \sum_{j=1}^{3} v_j^b \left(\mathbf{a}_i \cdot \mathbf{b}_j\right).$$

By defining $\mathbf{R}_b^a = \mathbf{a}_i \cdot \mathbf{b}_j$ and recalling the rules for matrix multiplication, the following compact form can be formulated

$$\mathbf{v}^a = \mathbf{R}_b^a \mathbf{v}^b. \tag{1}$$

It can be proven that the rotation matrix has the property that $\mathbf{R}_{a}^{b} = (\mathbf{R}_{b}^{a})^{-1} = (\mathbf{R}_{b}^{a})^{T}$ and $\det\mathbf{R}_{a}^{b} = 1$ [5]. The inverse of the rotation matrix being equal to its transpose is a very useful property as it allows the inverse matrix to be calculated without actually performing its calculation. The rotation matrix belongs to the special orthogonal group denoted SO(3) which uniquely has these properties.

An important property of the rotation matrix that was useful in the work of this thesis is that composite rotations can be described by multiplying simpler rotation matrices together. Then, this matrix multiplication can be represented by a single rotation matrix. More succinctly, this can be written as

$$\mathbf{v}^{c} = \mathbf{R}_{b}^{c}\mathbf{R}_{a}^{b}v^{a}, \tag{2}$$

where

$$\mathbf{R}_{a}^{c} = \mathbf{R}_{b}^{c}\mathbf{R}_{a}^{b}. \tag{3}$$

2.2.2 Euler Parameters

For terrestrial applications where large rotations are not encountered, Euler angles are often used to represent attitude. They have the advantage of being intuitively. However, for space applications where there is no bound for rotation, the Euler angle parameterization leads to singularities and requires reformulation of its representation as the spacecraft rotates. For numerical integration of the dynamics of a spacecraft, the use of Euler angles to represent a spacecraft's attitude presents a problem, as it is certain that the spacecraft will rotate through a singularity. To circumvent this limitation, Euler parameters or quaternions were chosen to represent the spacecraft's attitude as they are a global representation and do not contain any singularities [5]. In NADDS, the Euler parameter representation is used and is transparent to the user as the quaternion is transformed into a rotation matrix.

Any rotation of a rigid body can be represented as a rotation of an angle $\boldsymbol{\theta}$ about an axis $\mathbf{e}$, called the Euler axis [5]. When describing the rotation between two coordinate frames, this axis is common to both, which is defined as

$$\mathbf{e} = \mathrm{e}_1\mathbf{a}_1 + \mathrm{e}_2\mathbf{a}_2 + \mathrm{e}_3\mathbf{a}_3 = \mathrm{e}_1\mathbf{b}_1 + \mathrm{e}_2\mathbf{b}_2 + \mathrm{e}_3\mathbf{b}_3,$$

where e_i are the direction cosines of the Euler axis relative to coordinate frames A and B. From here, four Euler parameters can be defined as the following:

$$\mathrm{q}_1 = \mathrm{e}_1 \sin\left(\frac{\theta}{2}\right) \tag{4}$$

$$\mathrm{q}_2 = \mathrm{e}_2 \sin\left(\frac{\theta}{2}\right)$$

$$\mathrm{q}_3 = \mathrm{e}_3 \sin\left(\frac{\theta}{2}\right)$$

$$\mathrm{q}_4 = \cos\left(\frac{\theta}{2}\right)$$

Using some trigonometry, we note that the Euler parameters are constrained by

$$\mathbf{q}^\mathrm{T}\mathbf{q} + \mathrm{q}_4^2 = \mathrm{q}_1^2 + \mathrm{q}_2^2 + \mathrm{q}_3^2 + \mathrm{q}_4^2 = 1. \tag{5}$$

The rotation matrix from a reference frame A to another frame B can be parameterized in terms of quaternions:

$$\mathbf{R}_\mathrm{a}^\mathrm{b} = \begin{bmatrix} 1-2(\mathrm{q}_2^2+\mathrm{q}_3^2) & 2(\mathrm{q}_1\mathrm{q}_2+\mathrm{q}_3\mathrm{q}_4) & 2(\mathrm{q}_1\mathrm{q}_3-\mathrm{q}_2\mathrm{q}_4) \\ 2(\mathrm{q}_2\mathrm{q}_1-\mathrm{q}_3\mathrm{q}_4) & 1-2(\mathrm{q}_1^2+\mathrm{q}_3^2) & 2(\mathrm{q}_2\mathrm{q}_3+\mathrm{q}_1\mathrm{q}_4) \\ 2(\mathrm{q}_3\mathrm{q}_1+\mathrm{q}_2\mathrm{q}_4) & 2(\mathrm{q}_3\mathrm{q}_2-\mathrm{q}_1\mathrm{q}_4) & 1-2(\mathrm{q}_1^2+\mathrm{q}_2^2) \end{bmatrix}, \tag{6}$$

which can be represented more compactly if we define a skew symmetric matrix Q as

$$\mathbf{Q} = \begin{bmatrix} 0 & -\mathrm{q}_3 & \mathrm{q}_2 \\ \mathrm{q}_3 & 0 & -\mathrm{q}_1 \\ -\mathrm{q}_2 & \mathrm{q}_1 & 0 \end{bmatrix}.$$

Then we can rewrite the formulation for the rotation matrix in a more compact form,

$$\mathbf{R}_{\mathrm{a}}^{\mathrm{b}} = (\mathrm{q}_4^2 - \mathbf{q}^{\mathrm{T}}\mathbf{q})\mathrm{I} + 2\mathbf{q}\mathbf{q}^{\mathrm{T}} - 2\mathrm{q}_4\mathbf{Q}. \tag{7}$$

2.2.3. Quaternion Kinematics

It is simple to propagate the satellite's attitude given the inertial angular velocity of the satellite using quaternions. As derived in [5], the kinematic differential equation for the quaternion is as follows:

$$\dot{\mathbf{q}} = \frac{1}{2}(\mathrm{q}_4\boldsymbol{\omega} - \boldsymbol{\omega}\times\mathbf{q}) \tag{8}$$

$$\dot{\mathrm{q}_4} = -\frac{1}{2}\boldsymbol{\omega}^{\mathrm{T}}\mathbf{q},$$

where the attitude quaternion vector is $\mathbf{q} = [\mathrm{q}_1\ \mathrm{q}_2\ \mathrm{q}_3]^{\mathrm{T}}$ and the angular velocity of the satellite is $\omega=[\omega_1\ \omega_2\ \omega_3]^{\mathrm{T}}$,

$$\boldsymbol{\omega}\times\mathbf{q} = \begin{bmatrix} 0 & -\omega_3 & \omega_2 \\ \omega_3 & 0 & -\omega_1 \\ -\omega_2 & \omega_1 & 0 \end{bmatrix}\begin{bmatrix} \mathrm{q}_1 \\ \mathrm{q}_2 \\ \mathrm{q}_3 \end{bmatrix}. \tag{9}$$

For strapdown inertial reference systems for space vehicles, the body rates, ω, are measured and the kinematic differential equations, (8) and (9) are integrated numerically. Quaternions have no geometric singularity like Euler angles do and are well suited for onboard real-time computation because only products exist in the quaternion kinematic differential equation.

2.3 Frame Transformations

2.3.1 ECEF to ECI frame

To transform a vector in the Earth-Centered Inertial (ECI) coordinate frame to the Earth-Centered, Earth-Fixed (ECEF) the following transformation is performed:

$$\begin{bmatrix} \mathrm{e}_1 \\ \mathrm{e}_2 \\ \mathrm{e}_3 \end{bmatrix} = \begin{bmatrix} \cos\theta & \sin\theta & 0 \\ -\sin\theta & \cos\theta & 0 \\ 0 & 0 & 1 \end{bmatrix}\begin{bmatrix} \mathrm{i}_1 \\ \mathrm{i}_2 \\ \mathrm{i}_3 \end{bmatrix},$$

where e_1, e_2, and e_3 are the components of the vector in the ECEF frame and i_1, i_2, and i_3 are the components of the vector in the ECI frame [6].

Since the transformation matrix from the ECEF to ECI frame is important, we note that we can easily calculate $\mathbf{R}_{\mathrm{I}}^{\mathrm{E}}$ by taking the transpose of $\mathbf{R}_{\mathrm{E}}^{\mathrm{I}}$,

$$\mathbf{R}_{\mathrm{I}}^{\mathrm{E}} = \begin{bmatrix} \cos\theta & \sin\theta & 0 \\ -\sin\theta & \cos\theta & 0 \\ 0 & 0 & 1 \end{bmatrix}. \tag{10}$$

From inspection of (10), one can see that the third basis, or z-axis direction, of the ECI and ECEF coordinate frames coincide and that the ECEF coordinate frame is just a clockwise rotation about this rotation axis by the Earth rotation angle, θ. The ECI frame is considered inertially fixed such that the i_1 basis direction points towards the vernal equinox. The ECEF basis direction, $\mathbf{e}_1$, and consequently the $\mathbf{e}_2$ base direction, is fixed to the Earth and points at the prime meridian at all times [6].

To calculate θ, the time in Universal Time (UT) must be calculated first and converted to Greenwich Mean Sidereal Time (GMST). This time is the mean sidereal time at zero longitude. A common way that this is done is outlined in [7] and is repeated here

$$d_{2000} = 367y - \mathrm{INT}\left\{\frac{7\left\{y + \mathrm{INT}\left[\frac{m+9}{12}\right]\right\}}{4}\right\} + \mathrm{INT}\left\{\frac{275m}{9}\right\} + \frac{h + \frac{min}{60} + \frac{s}{3600}}{24} + d - 730531.5,$$

where d_{2000} are the fractional days past or before the beginning of year 2000, given the UT year y; month, m; day, d; hour, h; minute, min; and second, s. Here, INT is the truncation operation to the previous integer. The time in GMST has a one-to-one relationship with the Earth rotation angle according to

$$\theta = 280.46061837 + 360.98564736628 \times d_{2000},$$

where θ is in units of degrees.

Since the magnetic field given by the IGRF model gives a vector in the ECEF frame, it is important to use the rotation matrix from the ECEF to ECI frame to rotate the magnetic field vector from the ECEF frame to the ECI frame for the attitude determination calculations.

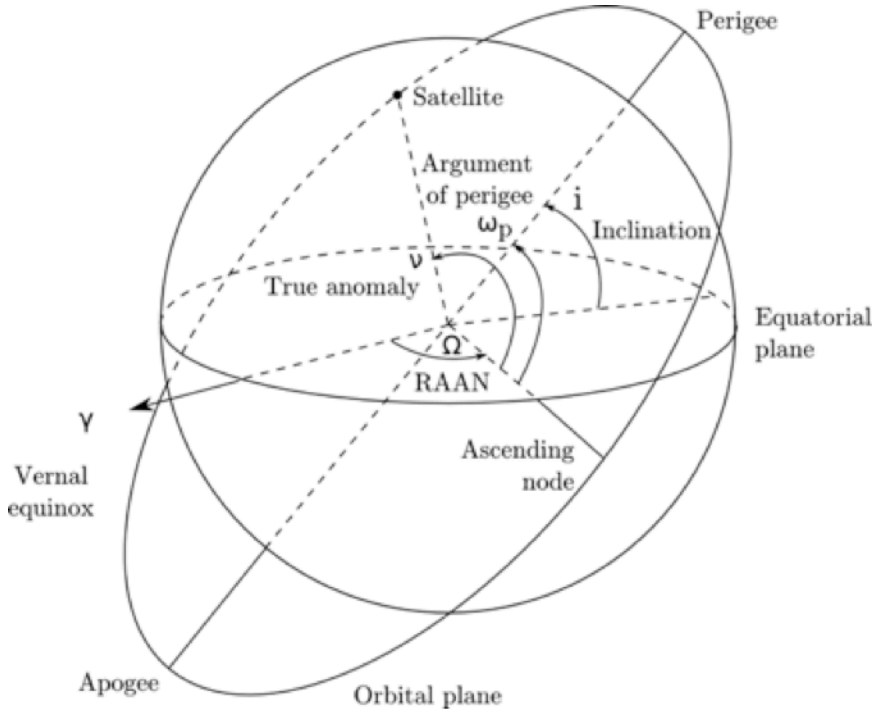

Figure 6: The orbital elements.

2.3.2 ECI to LVLH Frame

As described in [8], to transform from the ECI frame to the Local Vertical/Local Horizontal (LVLH) frame, three elementary rotations are performed. Referring to Figure 6, the first step is to rotate the coordinate frame by the RAAN, Ω. Then the coordinate frame is inclined about its x-axis by the inclination, i. Last, the coordinate frame is rotated by the argument of latitude, u. This is described mathematically as the following sequence of elementary rotations,

$$\mathbf{R}_{\mathrm{I}}^{\mathrm{L}} = \mathrm{ROT3(u)ROT1(i)ROT3}(\Omega),$$

where ROT3 is a rotation about the z-axis of the parent coordinate system and ROT1 is a rotation about the x-axis of the coordinate frame. Mathematically,

$$\mathrm{ROT3}(\cdot) = \begin{bmatrix} \cos(\cdot) & \sin(\cdot) & 0 \\ -\sin(\cdot) & \cos(\cdot) & 0 \\ 0 & 0 & 1 \end{bmatrix} \text{ and } \mathrm{ROT1}(\cdot) = \begin{bmatrix} 1 & 0 & 0 \\ 0 & \cos(\cdot) & \sin(\cdot) \\ 0 & -\sin(\cdot) & \cos(\cdot) \end{bmatrix}.$$

Using $\cos(\cdot) = \mathrm{c}(\cdot)$ and $\sin(\cdot) = \mathrm{s}(\cdot)$ to simplify the notation:

$$\mathrm{R}_{\mathrm{I}}^{\mathrm{L}} = \begin{bmatrix} \mathrm{c(u)} & \mathrm{s(u)} & 0 \\ -\mathrm{s(u)} & \mathrm{c(u)} & 0 \\ 0 & 0 & 1 \end{bmatrix} \begin{bmatrix} 1 & 0 & 0 \\ 0 & \mathrm{c(i)} & \mathrm{s(i)} \\ 0 & -\mathrm{s(i)} & \mathrm{c(i)} \end{bmatrix} \begin{bmatrix} \mathrm{c}(\Omega) & \mathrm{s}(\Omega) & 0 \\ -\mathrm{s}(\Omega) & \mathrm{c}(\Omega) & 0 \\ 0 & 0 & 1 \end{bmatrix} \tag{11}$$

$$= \begin{bmatrix} \mathrm{c}(\Omega)\mathrm{c(u)} - \mathrm{c(i)s}(\Omega)\mathrm{s(u)} & \mathrm{c(u)s}(\Omega) + \mathrm{c(i)c}(\Omega)\mathrm{s(u)} & \mathrm{s(i)s(u)} \\ -\mathrm{c}(\Omega)\mathrm{s(u)} - \mathrm{c(i)c(u)s}(\Omega) & \mathrm{c(i)c}(\Omega)\mathrm{c(u)} - \mathrm{s}(\Omega)\mathrm{s(u)} & \mathrm{c(u)s(i)} \\ \mathrm{s(i)s}(\Omega) & -\mathrm{c}(\Omega)\mathrm{s(i)} & \mathrm{c(i)} \end{bmatrix}$$

The perigee is the angle measured between the ascending node to the periapsis, which is the closest point to the Earth. For a perfectly circular orbit, the argument of perigee is undefined since there is no periapsis. In this case an alternate definition is used called the argument of latitude denoted by, u. The argument of latitude would require the satellite's position, $\mathbf{r}$, and the ascending node direction, $\mathbf{n}$, and the calculation would be

$$\cos(\mathrm{u}) = \frac{\mathbf{n} \cdot \mathbf{r}}{|\mathbf{n}||\mathbf{r}|}.$$

However, it is the position of the satellite that we are searching for, so we cannot calculate the argument of latitude in this fashion unless we knew when the satellite passed the ascending node direction. Ideally, we would like some form of relation that includes time. Fortunately for our orbit, there is a measureable periapsis so from the TLE, the argument of latitude can be calculated using

$$\mathrm{u} = \omega + \nu,$$

where ω is the argument of periapsis and ν is the true anamoly. The time of writing this report, the inclination, i, of H2's orbit is 40.5298 degrees, and the RAAN, Ω, is about 240.8768 degrees. The argument of perigee is given by the TLE as 12.2599 degrees at the time of 22.49945294 days into the 2014 year in UTC. To find the true anomaly the following calculation needs to be performed,

$$\nu = \frac{360^{\circ}}{2\pi}\frac{2\pi}{1\ \mathrm{rev}}(\mathrm{t} - \mathrm{t}_0)\omega_0, \tag{12}$$

where t is the current time in days and fraction thereof from the beginning of the year, t_0 is the epoch for the TLE and ω_0 is the mean motion of the satellite in rev/day. Since a satellite revolves around the Earth many times a day, this value needs to then be converted to be between 0 and 360 degrees using the mod operator that is common in most programming languages.

2.4 Attitude Determination

To determine H2's attitude, two reference vectors are required. Both reference vectors need to be measured by the attitude determination sensors as well and determined analytically through models. The measured set will be measured in the satellite's body frame while the analytical set can be modeled in other frame such as the ECI frame or the ECEF frame. In the case for this thesis, the Sun vector, $\mathbf{v}_\mathrm{S}$, and local magnetic field vector, $\mathbf{v}_\mathrm{M}$, are both measured and calculated analytically.

2.4.1 Sun Sensor Model

Assuming that there is a photodiode on each of the faces of a satellite, who's short-circuit current is measured, then the model for the Sun sensor is

$$\mathrm{i}_\mathrm{i} = \begin{cases} \hat{\mathbf{v}}_\mathrm{S}^\mathrm{B} \cdot \hat{\mathbf{n}}_\mathrm{i} + \eta_\mathrm{s} & \text{if } \hat{\mathbf{v}}_\mathrm{S}^\mathrm{B} \cdot \hat{\mathbf{n}}_\mathrm{i} > 0 \\ 0 & \text{otherwise} \end{cases} \tag{13}$$

where $\hat{\mathbf{v}}_\mathrm{S}^\mathrm{B}$ is the unit vector in the spacecraft's body frame pointing from the spacecraft center of mass to the Sun, $\hat{\mathbf{n}}_\mathrm{i}$ is the unit vector for face i, η_s is a sample from the normal distribution, $\mathcal{N}(0, \sigma_\mathrm{s}^2)$. The standard deviation of the

current noise, σ_s , is assumed to be 100 uA. There are a total of six photodiodes used on H2. The Sun sensor vector is then formed according to

$$\hat{\mathbf{r}}_{sun} = \frac{\sum_{i=1}^{n} i_i \hat{\mathbf{n}}_i}{\sqrt{\sum_{i=1}^{n} i_i^{\,2}}},$$

where n is the number of current measurements. The currents follow this relation when the spacecraft is in the Sun; however, when in the eclipse, all the photodiode currents are assumed to be zero.

2.4.2 Eclipse Calculation

A simple geometrical method is used to determine whether or not H2 is in the eclipse (Fig. 7). An algorithm from [9] was used (Table 1).

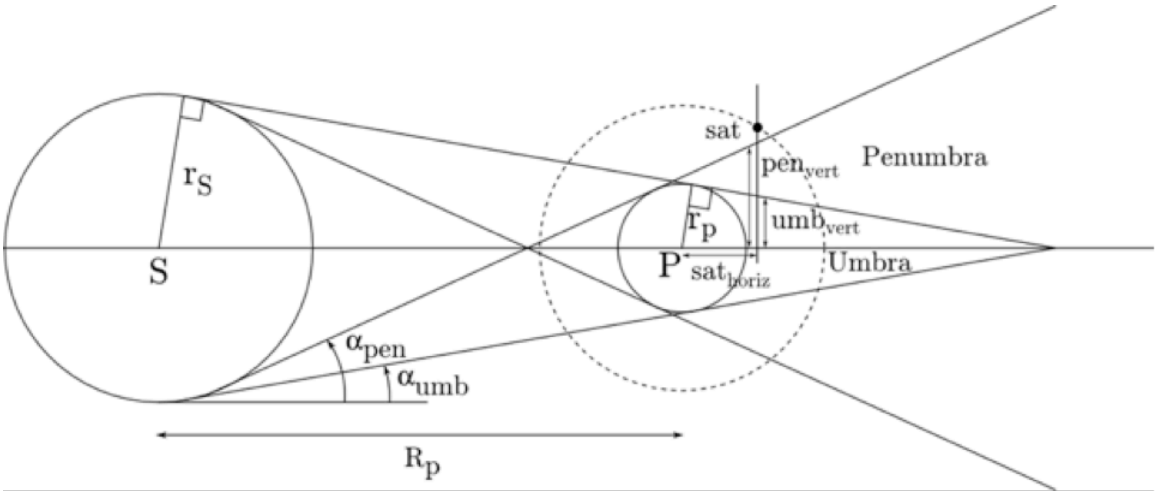

Figure 7: The geometry used for eclipse determination.

Here $\alpha_{umb}$is the angle between the horizontal and a ray drawn between the circumference of the Sun to the circumference on the same side of the Earth and $\alpha_{pen}$is the angle between the horizontal and a ray drawn between the circumference of the Sun to the Earth, but on the opposite side. The radius of the Sun is r_s and the radius of the Earth is denoted as r_p. The distance between the Earth and Sun is R_p. The Sun direction in the inertial frame is $\mathbf{v}_S^I$ and the position of the satellite in the inertial frame is $\mathbf{v}_P^I$. SAT_{horiz} is the horizontal component of the distance drawn between the Earth center and the satellite. SAT_{vert} is the

vertical component of distance drawn between the center of the Earth and the satellite. $\mathrm{PEN}_{\mathrm{vert}}$ is the penumbra vertical component and $\mathrm{UMB}_{\mathrm{vert}}$ is the vertical component of the umbra. For simplicity, if it is determined that the satellite is in either the penumbra or umbra regions, the solar irradiance on the satellite is assumed to be zero. Otherwise, it is assumed to be $1367\ \mathrm{W/m^2}$.

Table 1: The eclipse determination algorithm.

$$\tan(\alpha_{\mathrm{umb}}) = \frac{r_s - r_p}{R_p} = \frac{696000 - 6378}{149599870} \Rightarrow \alpha_{\mathrm{umb}} = 0.264°$$

$$\tan(\alpha_{\mathrm{pen}}) = \frac{r_s + r_p}{R_p} = \frac{696000 + 6378}{149599870} \Rightarrow \alpha_{\mathrm{pen}} = 0.269°$$

shadow='none'.
if $\left(\mathbf{v}_S^I \cdot \mathbf{v}_P^I\right) < 0$
$\varsigma = \mathrm{acos}\left(\frac{-\mathbf{v}_S^I \cdot \mathbf{v}_P^I}{\left|\mathbf{v}_S^I\right|\left|\mathbf{v}_P^I\right|}\right)$
$\mathrm{SAT}_{\mathrm{horiz}} = \left|\mathbf{v}_P^I\right|\cos(\varsigma)$
$\mathrm{SAT}_{\mathrm{vert}} = \left|\mathbf{v}_P^I\right|\sin(\varsigma)$
$\mathrm{PEN}_{\mathrm{vert}} = R_{\oplus} + \tan(\alpha_{\mathrm{pen}})\mathrm{SAT}_{\mathrm{horiz}}$
if $\mathrm{SAT}_{\mathrm{vert}} \leq \mathrm{PEN}_{\mathrm{vert}}$
shadow='penumbra'
$\mathrm{UMB}_{\mathrm{vert}} = R_{\oplus} + \tan(\alpha_{\mathrm{umb}})\mathrm{SAT}_{\mathrm{horiz}}$
if $\mathrm{SAT}_{\mathrm{vert}} \leq \mathrm{UMB}_{\mathrm{vert}}$
shadow='umbra'

2.4.3 Magnetometer Model

The measurement model for magnetometer is

$$\mathbf{v}_{\mathrm{M,MEAS}}^{\mathrm{B}} = \mathbf{v}_{\mathrm{M,TRUE}}^{\mathrm{B}} + \boldsymbol{\eta}_{\mathbf{M}} \tag{14}$$

where $\mathbf{v}_{\mathrm{M,MEAS}}^{\mathrm{B}}$ is the simulated measurement of magnetic field vector by the magnetometer based on the IGRF model solution, $\mathbf{v}_{\mathrm{M,TRUE}}^{\mathrm{B}}$, and $\boldsymbol{\eta}_{\mathbf{M}}$ is the normal distribution vector, $\mathcal{N}(\mathbf{0}, \sigma_M^2\mathbf{I})$ representing noise in the measurement. It is traditional for the noise in the measurement to be proportional to the magnitude

of the magnetic field, however the magnetic field strength is close to constant since H2's orbit does not pass close to the poles, therefore the magnitude of the standard deviation is not assumed to change as the satellite travels in its orbit. The standard deviation of the error for the magnetometer readings, σ_{M}, on each axis is assumed to be approximately 2 mG [10].

2.4.4 Sun Position in the ECI Frame

The algorithm to calculate the Sun vector in the ECI frame is found in [9]. The first step is to calculate the Julian date. This is done using:

$$\mathrm{JD} = 367(\mathrm{year}) - \mathrm{INT}\left\{\frac{7\left[\mathrm{year} + \mathrm{INT}\left(\frac{\mathrm{month}+9}{12}\right)\right]}{4}\right\} + \mathrm{INT}\left(\frac{275(\mathrm{month})}{9}\right) + \mathrm{day} + 1{,}721{,}013.5 + \frac{\mathrm{hour}}{24} + \frac{\mathrm{minute}}{1440} + \frac{\mathrm{second}}{86{,}400},$$

where the year, month, day, hour, minute, and second are expressed in UTC.

The universal time, $\mathrm{T_{UT}}$, is calculated as:

$$\mathrm{T_{UT}} = \frac{\mathrm{JD} - 2{,}451{,}545.0}{36{,}525}$$

where $\mathrm{T_{UT}}$ is in centuries.

The mean longitude of the Sun, $\lambda_{\mathrm{M,sun}}$, can be calculated in units of degrees,

$$\lambda_{\mathrm{M,Sun}} = 280.4606184^{\circ} + 36{,}000.77005361\mathrm{T_{UT}}.$$

The mean anomaly, $\mathrm{M_{Sun}}$, also in degrees, is then

$$\mathrm{M_{Sun}} = 357.5277233^{\circ} + 35{,}999.05034\mathrm{T_{UT}}.$$

The ecliptic longitude of the Sun, $\lambda_{\mathrm{ecliptic}}$, in degrees is then

$$\lambda_{\mathrm{ecliptic}} = \lambda_{\mathrm{M,Sun}} + 1.914666471^{\circ}\sin(\mathrm{M_{Sun}}) + 0.918994643^{\circ}\sin(2\mathrm{M_{Sun}}).$$

And the obliquity of the ecliptic, ε , in degrees is

$$\varepsilon = 23.439291^{\circ} - 0.0130042\mathrm{T}_{\mathrm{TDB}}.$$

Since only direction information is required for attitude estimation, the astronomical units are stripped away and the Sun position vector in the ECI frame becomes

$$\hat{\mathbf{v}}_{\mathrm{S}}^{\mathrm{I}} = \begin{bmatrix} \cos\lambda_{\mathrm{ecliptic}} \\ \sin\lambda_{\mathrm{ecliptic}}\cos\varepsilon \\ \sin\lambda_{\mathrm{ecliptic}}\sin\varepsilon \end{bmatrix} \tag{15}$$

2.4.5 Magnetic Field Model in ECEF

To determine the magnetic field local to the position of the satellite, the eleventh generation International Geomagnetic Reference Field (IGRF) model (2010 version) was used. The magnetic field of Earth roughly resembles that of a large dipole magnet and can vary from 30000 nT at the equator to 60000 nT near the poles. Within several Earth radii, the IGRF model has accuracies of a few tens of nT therefore can be regarded as a very accurate model for Earth's magnetic field for LEO [11].

The IGRF model was created by the International Association of Geomagnetism and Aeronomy (IAGA) and it uses a set of Gaussian coefficients, $\mathrm{g}_{\mathrm{n}}^{\mathrm{m}}$ and $\mathrm{h}_{\mathrm{n}}^{\mathrm{m}}$ in a spherical harmonic model to approximate the Earth's magnetic field. The coefficients are updated every five years. The field is described as the negative gradient of the potential function that is modeled by spherical harmonics

$$\begin{aligned} \mathrm{B} &= -\nabla \mathrm{V}(\mathrm{R}_{\mathrm{c}}, \lambda', \theta) \\ &= \nabla \left\{ \mathrm{R}_{\mathrm{e}} \sum_{\mathrm{n}=1}^{\mathrm{k}} \left(\frac{\mathrm{R}_{\mathrm{e}}}{\mathrm{R}_{\mathrm{c}}}\right)^{\mathrm{n}+1} \sum_{\mathrm{m}=0}^{\mathrm{n}} \left[\mathrm{g}_{\mathrm{n}}^{\mathrm{m}} \cos(\mathrm{m}\theta) + \mathrm{h}_{\mathrm{n}}^{\mathrm{m}} \sin(\mathrm{m}\theta)\right] \mathrm{P}_{\mathrm{n}}^{\mathrm{m}}(\lambda') \right\}, \end{aligned}$$

where R_{e} is the Earth radius, R_{c}, is the distance from the center of the Earth to the center of the spacecraft, and $\mathrm{P}_{\mathrm{n}}^{\mathrm{m}}(\lambda')$ is the Schmidt normalized associated

Legendre polynomials, θ is the longitude of the spacecraft, and λ' is the co-latitude of the satellite. Taking the gradient of $V(R_c, \lambda', \theta)$ gives the magnetic field vector components in the ECEF frame at the location (R_c, λ', θ) coordinate triple in spherical coordinates. The equations for the three components are:

$$B_r = -\frac{\partial V}{\partial R_c} = \sum_{n=1}^{k} \left(\frac{R_e}{R_c}\right)^{n+2} (n+1) \sum_{m=0}^{n} [g^{m,n}\cos(m\theta) + h^{n,m}\sin(m\theta)]\, P_n^m(\lambda')$$

$$B_{\lambda'} = \frac{1}{-R_c}\frac{\partial V}{\partial \lambda'} = -\sum_{n=1}^{k} \left(\frac{R_e}{R_c}\right)^{n+2} \sum_{m=0}^{n} [g^{m,n}\cos(m\theta) + h^{n,m}\sin(m\theta)]\, \frac{\partial P_n^m(\lambda')}{\partial \lambda'}$$

$$B_\theta = -\frac{1}{R_c \sin(\lambda')}\frac{\partial V}{\partial \lambda'}$$

$$= -\frac{1}{\sin(\lambda')} \sum_{n=1}^{k} \left(\frac{R_e}{R_c}\right)^{n+2} \sum_{m=0}^{n} m[-g^{m,n}\sin(m\theta) + h^{n,m}\sin(m\theta)]\, P_n^m(\lambda')$$

As one can see immediately, this model is complex and is well out of the scope of this project, so it is left up to the reader to refer to [12] if a deeper understanding is desired. For the purposes of this thesis, it suffices to say that the dipole-shaped field is not trivial. It is for this reason that a MATLAB routine developed at NASA, available at [13], was adapted for use in the NADDS to perform the magnetic field calculations.

The calculation of the local magnetic field directly using the general IGRF model is computationally expensive, such that it would be difficult for a weak processor onboard a CubeSat to perform this calculation in real time. It is more computationally efficient to generate a grid of pre-calculated values for the magnetic field and use interpolation to calculate the local magnetic field using the satellite's orbit position [14]. To do this, a grid of latitude and longitudes were mapped on a sphere around the Earth at an altitude of 500 km. The grid spacing was set to 10 degrees in both latitude and longitude, thus creating a grid of 648 points. At each of these points, the magnetic field in the ECEF basis directions was calculated. The interpolation was done in polar coordinates, and the satellite was assumed to be at exactly 500 km altitude. Since the magnetic field vector

has three components in the ECEF, three lookup tables were created for the interpolation.

Since the interpolation is done in two dimensions, two interpolations must be done. The first interpolation creates an array of vectors that is the magnetic field directions for the latitude of the satellite, but still at all possible longitudes. Then the array of vectors is interpolated at the longitude of the satellite.

Table 2: The magnetic field interpolation algorithm.

1. Read IGRF X, Y, and Z lookup tables.
2. Read in latitude and longitude of desired location.
3. Search for two columns that straddle the desired latitude in each of the X, Y, and Z lookup tables.
4. Interpolate at each of the lookup table's longitudes, the magnetic field strength at the input latitude using the two columns that straddle the desired latitude.
5. Repeat for the X, Y, and Z directions tables.
6. Form temporary vectors for the interpolated magnetic field strengths in the X, Y, and Z direction at the desired latitude and set of longitudes.
7. Within each of these vectors search for the latitudes that straddle the input latitude.
8. Interpolate for the X, Y, and Z magnetic field strength at the desired latitude and longitude.

Equations (16) and (17) were used for the interpolations.

$$\mathrm{v}_{\mathrm{M,i}}^{\mathrm{E}}(\mathrm{lat},\mathrm{long}) = \left(\frac{\mathrm{v}_{\mathrm{M,i}}^{\mathrm{E}}(\mathrm{j}+1) - \mathrm{v}_{\mathrm{M,i}}^{\mathrm{E}}(\mathrm{j})}{\mathrm{long}(\mathrm{j}+1) - \mathrm{long}(\mathrm{j})}\right)(\mathrm{inputlong} \quad - \mathrm{long}(\mathrm{j})) + \mathrm{v}_{\mathrm{M,i}}^{\mathrm{E}}(\mathrm{j}) \tag{16}$$

$$\mathrm{v}_{\mathrm{M,i}}^{\mathrm{E}}(\mathrm{lat},\mathrm{long}) = \left(\frac{\mathrm{v}_{\mathrm{M,i}}^{\mathrm{E}}(\mathrm{j}+1) - \mathrm{v}_{\mathrm{M,i}}^{\mathrm{E}}(\mathrm{j})}{\mathrm{lat}(\mathrm{j}+1) - \mathrm{lat}(\mathrm{j})}\right)(\mathrm{inputlat} \quad - \mathrm{lat}(\mathrm{j})) + \mathrm{v}_{\mathrm{M,i}}^{\mathrm{E}}(\mathrm{j}), \tag{17}$$

where $\mathrm{v}_{\mathrm{M,i}}^{\mathrm{E}}(\mathrm{lat},\mathrm{long})$ is the magnetic field strength in the ith direction at that longitude and latitude.

Error is introduced by interpolating the magnetic field since it is not computed exactly at the point of interest and it is important to characterize this source of

error. Errors will occur in both the magnitude and direction estimates; however, since the magnetic field is used for attitude determination, it is more important that the error in orientation of the magnetic field be characterized. This error is defined as the difference between the interpolated vector direction and the true vector direction calculated directly using the IGRF model (Fig. 8).

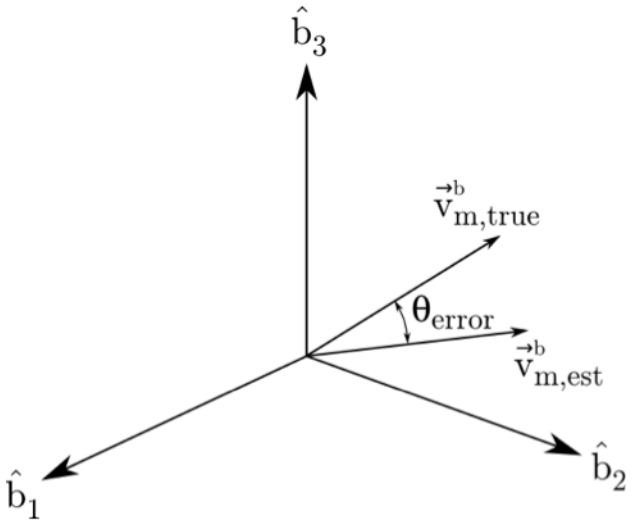

Figure 8: The error in the magnetic field estimate calculated in the satellite body frame.

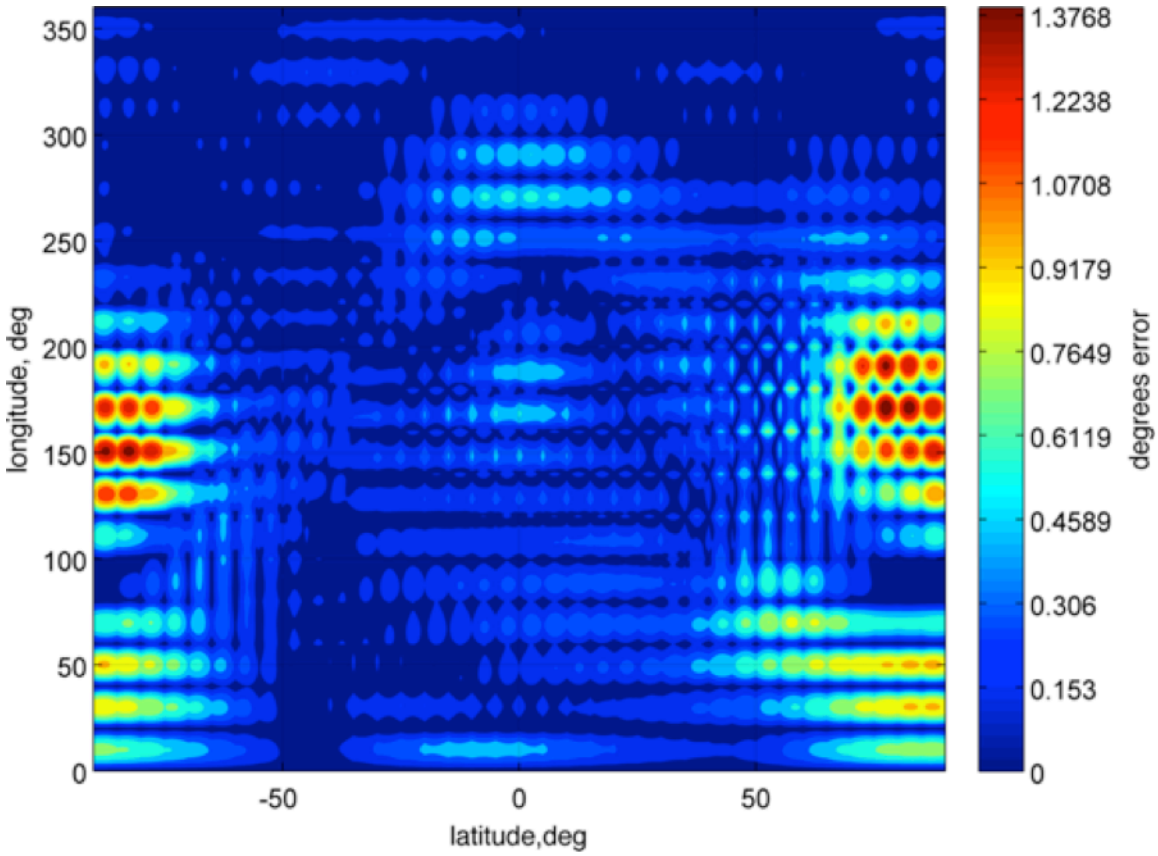

Figure 9: The interpolated magnetic field direction estimate error.

The maximum error that one can expect in the interpolation model is 1.5 degrees, but looking at Figure 9, we can see that most of the time the error is less than 1 degree. The error increases when the position is the vicinity of the poles since the field's curvature is greatest around the poles. Since H2's orbit has an inclination of 40.5 degrees, its latitude will not go past 40.5 degrees north or south of the equator. In that region, the error is less than 0.5 degrees. Plotting the error as a histogram and then integrating, Figure 10 shows the probability of the error being below a given threshold.

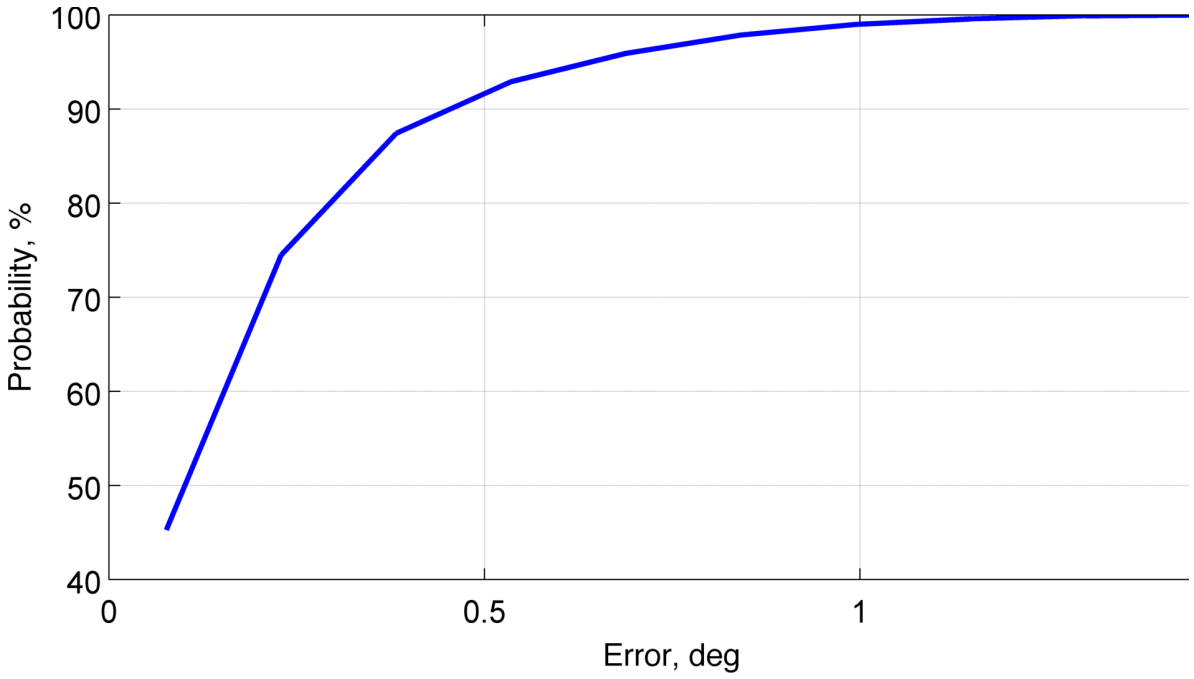

Figure 10: The probability that the true magnetic field direction is within a given error of the estimate.

In Figure 10, we see that there is nearly a 100% probability that any estimate of the magnetic field has a direction error of less than 1 degree. This suggests that the lookup tables can have a lower density than 10 degrees of latitude and longitude and still achieve accurate results in estimating the magnetic field direction. It is suspected that this low sensitivity in the magnetic field estimate error is due to the low inclination of the orbit.

2.4.5 TRIAD Estimation Scheme & Nadir Pointing Error

To estimate the attitude of a satellite, a minimum of two reference vectors are needed in two separate frames. The TRIaxial Attitude Determination (TRIAD) scheme is simple in that it is a deterministic attitude estimator that requires only two body frame sensor measurements and two measurements in another frame [15]. Such measurements could be magnetic field vectors and Sun vectors in the inertial frame and measured in the body frame.

The determination process begins by H2 measuring the magnetic field, $\mathbf{v}_{\mathrm{M}}^{\mathrm{B}}$, and Sun vector, $\mathbf{v}_{\mathrm{S}}^{\mathrm{B}}$, in its body frame using its magnetometer and photodiodes. Then the direction of the Sun in the inertial frame is calculated using (15) and using the GPS coordinate, the local magnetic field direction is calculated in the ECEF frame using the 2010 IGRF model. Like before, since we are interested in the attitude of the satellite, the magnitudes of these vectors are unimportant. Therefore, since only attitude information is desired, these four vectors are normalized

$$\hat{\mathbf{v}}_{\mathrm{M}}^{\mathrm{B}} = \frac{\mathbf{v}_{\mathrm{M}}^{\mathrm{B}}}{\sqrt{\mathbf{v}_{\mathrm{M}}^{\mathrm{B}}\mathbf{v}_{\mathrm{M}}^{\mathrm{B}\,\mathrm{T}}}}, \hat{\mathbf{v}}_{\mathrm{S}}^{\mathrm{B}} = \frac{\mathbf{v}_{\mathrm{S}}^{\mathrm{B}}}{\sqrt{\mathbf{v}_{\mathrm{S}}^{\mathrm{B}}\mathbf{v}_{\mathrm{S}}^{\mathrm{B}\,\mathrm{T}}}}, \hat{\mathbf{v}}_{\mathrm{S}}^{\mathrm{I}} = \frac{\mathbf{v}_{\mathrm{S}}^{\mathrm{I}}}{\sqrt{\mathbf{v}_{\mathrm{S}}^{\mathrm{I}}\mathbf{v}_{\mathrm{S}}^{\mathrm{I}\,\mathrm{T}}}}, \hat{\mathbf{v}}_{\mathrm{M}}^{\mathrm{E}} = \frac{\mathbf{v}_{\mathrm{M}}^{\mathrm{E}}}{\sqrt{\mathbf{v}_{\mathrm{M}}^{\mathrm{E}}\mathbf{v}_{\mathrm{M}}^{\mathrm{E}\,\mathrm{T}}}}.$$

The magnetic field vector is estimated in the ECEF frame, the GPS coordinate is already in the ECEF frame, however, the Sun vector is in the ECI frame. Therefore the magnetic field vector is transformed into the ECI frame by

$$\hat{\mathbf{v}}_{\mathrm{M}}^{\mathrm{I}} = \mathbf{R}_{\mathrm{E}}^{\mathrm{I}}\hat{\mathbf{v}}_{\mathrm{M}}^{\mathrm{E}} = \mathbf{R}_{\mathrm{I}}^{\mathrm{E}\,\mathrm{T}}\hat{\mathbf{v}}_{\mathrm{M}}^{\mathrm{E}}.$$

Now we have two sets of vectors one are measurements in the body frame of the spacecraft and the other are vectors in the ECEF frame. Each set contains a Sun vector and a magnetic field vector. We know that there exists an attitude transformation, $\mathbf{R}_{\mathrm{B}}^{\mathrm{I}}$, such that

$$\hat{\mathbf{v}}_{\mathrm{S}}^{\mathrm{I}} = \mathbf{R}_{\mathrm{B}}^{\mathrm{I}}\hat{\mathbf{v}}_{\mathrm{S}}^{\mathrm{B}} \text{ and } \hat{\mathbf{v}}_{\mathrm{M}}^{\mathrm{I}} = \mathbf{R}_{\mathrm{B}}^{\mathrm{I}}\hat{\mathbf{v}}_{\mathrm{M}}^{\mathrm{B}}.$$

Since $\hat{\mathbf{v}}_{\mathrm{S}}^{\mathrm{B}}$ and $\hat{\mathbf{v}}_{\mathrm{M}}^{\mathrm{B}}$ are linearly independent, the following relation is true

$$\hat{\mathbf{v}}_{\mathrm{S}}^{\mathrm{I}} \times \hat{\mathbf{v}}_{\mathrm{M}}^{\mathrm{I}} = \mathbf{R}_{\mathrm{B}}^{\mathrm{I}}(\hat{\mathbf{v}}_{\mathrm{S}}^{\mathrm{B}} \times \hat{\mathbf{v}}_{\mathrm{M}}^{\mathrm{B}}).$$

So we can say

$$\{\hat{\mathbf{v}}_{\mathrm{S}}^{\mathrm{I}} \quad \hat{\mathbf{v}}_{\mathrm{M}}^{\mathrm{I}} \quad \hat{\mathbf{v}}_{\mathrm{S}}^{\mathrm{I}} \times \hat{\mathbf{v}}_{\mathrm{M}}^{\mathrm{I}}\} = \mathbf{R}_{\mathrm{B}}^{\mathrm{I}}\{\hat{\mathbf{v}}_{\mathrm{S}}^{\mathrm{B}} \quad \hat{\mathbf{v}}_{\mathrm{M}}^{\mathrm{B}} \quad \hat{\mathbf{v}}_{\mathrm{S}}^{\mathrm{B}} \times \hat{\mathbf{v}}_{\mathrm{M}}^{\mathrm{B}}\}.$$

To solve for $\mathbf{R}_{\mathrm{B}}^{\mathrm{I}}$, $\{\hat{\mathbf{v}}_{\mathrm{S}}^{\mathrm{B}} \quad \hat{\mathbf{v}}_{\mathrm{M}}^{\mathrm{B}} \quad \hat{\mathbf{v}}_{\mathrm{S}}^{\mathrm{B}} \times \hat{\mathbf{v}}_{\mathrm{M}}^{\mathrm{B}}\}$ can be inverted by a brute force method. However, if we make the following adjustments,

$$\mathbf{A}_1 = \left\{ \hat{\mathbf{v}}_{\mathrm{S}}^{\mathrm{I}} \quad \frac{\hat{\mathbf{v}}_{\mathrm{S}}^{\mathrm{I}} \times \hat{\mathbf{v}}_{\mathrm{M}}^{\mathrm{I}}}{\left| \hat{\mathbf{v}}_{\mathrm{S}}^{\mathrm{I}} \times \hat{\mathbf{v}}_{\mathrm{M}}^{\mathrm{I}} \right|} \times \hat{\mathbf{v}}_{\mathrm{S}}^{\mathrm{I}} \quad \hat{\mathbf{v}}_{\mathrm{S}}^{\mathrm{I}} \times \hat{\mathbf{v}}_{\mathrm{M}}^{\mathrm{I}} \right\} = \mathbf{R}_{\mathrm{B}}^{\mathrm{I}} \mathbf{A}_2$$

$$= \mathbf{R}_{\mathrm{B}}^{\mathrm{I}} \left\{ \hat{\mathbf{v}}_{\mathrm{S}}^{\mathrm{B}} \quad \frac{\hat{\mathbf{v}}_{\mathrm{S}}^{\mathrm{B}} \times \hat{\mathbf{v}}_{\mathrm{M}}^{\mathrm{B}}}{\left| \hat{\mathbf{v}}_{\mathrm{S}}^{\mathrm{B}} \times \hat{\mathbf{v}}_{\mathrm{M}}^{\mathrm{B}} \right|} \times \hat{\mathbf{v}}_{\mathrm{S}}^{\mathrm{B}} \quad \hat{\mathbf{v}}_{\mathrm{S}}^{\mathrm{B}} \times \hat{\mathbf{v}}_{\mathrm{M}}^{\mathrm{B}} \right\},$$

we find that $\mathbf{A}_1$ and $\mathbf{A}_2$ become orthogonal and that $\mathbf{A}_2$ can be inverted by a simple transpose. So

$$\mathbf{R}_{\mathrm{B}}^{\mathrm{I}} = \left\{ \hat{\mathbf{v}}_{\mathrm{S}}^{\mathrm{I}} \quad \frac{\hat{\mathbf{v}}_{\mathrm{S}}^{\mathrm{I}} \times \hat{\mathbf{v}}_{\mathrm{M}}^{\mathrm{I}}}{\left| \hat{\mathbf{v}}_{\mathrm{S}}^{\mathrm{I}} \times \hat{\mathbf{v}}_{\mathrm{M}}^{\mathrm{I}} \right|} \times \hat{\mathbf{v}}_{\mathrm{S}}^{\mathrm{I}} \quad \hat{\mathbf{v}}_{\mathrm{S}}^{\mathrm{I}} \times \hat{\mathbf{v}}_{\mathrm{M}}^{\mathrm{I}} \right\} \left\{ \hat{\mathbf{v}}_{\mathrm{S}}^{\mathrm{B}} \quad \frac{\hat{\mathbf{v}}_{\mathrm{S}}^{\mathrm{B}} \times \hat{\mathbf{v}}_{\mathrm{M}}^{\mathrm{B}}}{\left| \hat{\mathbf{v}}_{\mathrm{S}}^{\mathrm{B}} \times \hat{\mathbf{v}}_{\mathrm{M}}^{\mathrm{B}} \right|} \times \hat{\mathbf{v}}_{\mathrm{S}}^{\mathrm{B}} \quad \hat{\mathbf{v}}_{\mathrm{S}}^{\mathrm{B}} \times \hat{\mathbf{v}}_{\mathrm{M}}^{\mathrm{B}} \right\}^{\mathrm{T}}. \tag{18}$$

$\mathbf{R}_{\mathrm{B}}^{\mathrm{I}}$ is the rotation matrix that transforms a vector in the body frame into a vector in the inertial frame, which ultimately is the task of the TRIAD estimator.

Let us assume for simplicity that we have a reliable GPS lock and can get position estimates at any time that we want. The GPS position is defined in the ECEF frame and it is desired to transform this into the ECI frame,

$$\mathbf{v}_{\mathrm{P}}^{\mathrm{I}} = {\mathbf{R}_{\mathrm{I}}^{\mathrm{E}}}^{\mathrm{T}} \mathbf{v}_{\mathrm{P}}^{\mathrm{E}}.$$

Then the position vector is transformed into the body frame,

$$\mathbf{v}_{\mathrm{P}}^{\mathrm{B}} = {\mathbf{R}_{\mathrm{B}}^{\mathrm{I}}}^{\mathrm{T}} \mathbf{v}_{\mathrm{P}}^{\mathrm{I}}.$$

Note that the position vector of the satellite is antiparallel to the nadir direction, so

$$\mathbf{v}_{\mathrm{N}}^{\mathrm{I}} = -\mathbf{v}_{\mathrm{P}}^{\mathrm{I}} = -{\mathbf{R}_{\mathrm{B}}^{\mathrm{I}}}^{\mathrm{T}} \mathbf{v}_{\mathrm{P}}^{\mathrm{I}}$$

Again, the magnitude is irrelevant for attitude information, so we normalized this vector

$$\hat{\mathbf{v}}_{\mathrm{N}}^{\mathrm{I}} = \frac{\mathbf{v}_{\mathrm{N}}^{\mathrm{B}}}{\sqrt{\mathbf{v}_{\mathrm{N}}^{\mathrm{B}\,\mathrm{T}}\mathbf{v}_{\mathrm{N}}^{\mathrm{B}}}}.$$

The $-\mathrm{e}_3$ body frame axis runs parallel to the axis of the transponder antenna. So to define a nadir pointing error angle, this angle would be between the transponder antenna pointing direction and the nadir vector. Both are in the body frame; therefore, we can define the dot product as

$$\hat{\mathbf{v}}_{\mathrm{N}}^{\mathrm{B}} \cdot (-\mathrm{e}_3) = \left\|\hat{\mathbf{v}}_{\mathrm{N}}^{\mathrm{B}}\right\| \|\mathrm{e}_3\| \cos\alpha_{\mathrm{nadir}} = \cos\alpha_{\mathrm{nadir}}.$$

Solving for the nadir pointing error,

$$\begin{aligned} \alpha_{\mathrm{nadir}} &= \cos^{-1}\left(\hat{\mathbf{v}}_{\mathrm{N}}^{\mathrm{B}} \cdot (-\mathrm{e}_3)\right) \\ &= \cos^{-1}\left(-\hat{\mathrm{v}}_{\mathrm{N},3}^{\mathrm{B}}\right), \end{aligned} \tag{19}$$

one can see that from (19) that α_{nadir} tends to zero as the unit vector of the nadir direction in the body frame rotates to the $-\mathrm{e}_3$ axis of the spacecraft.

2.5 Control & Disturbance Torques

H2 has magnetic torque coils and a gravity-gradient boom as control actuators. The magnetic torque coils are an active control element whereas the gravity gradient boom is passive. Although the gravity gradient provides the potential energy field that orients the satellite such that it points nadir, the gravity-gradient torque is conservative and without a form of dissipation, H2 would oscillate indefinitely. Therefore, the magnetic torque coils play a critical role in achieving the nadir pointing orientation. Since the spacecraft is in low Earth orbit, the aerodynamic drag on the satellite is significant when the gravity-gradient boom is deployed such that it must be accounted for. The torques provided by these actuators and the disturbance torque due to aerodynamic drag will be discussed in this section.

2.5.1 Satellite Dynamics Model

For a rigid body such as a satellite in orbit around the Earth, the dynamics of the motion is

$$\mathbf{J}\dot{\boldsymbol{\omega}} = \mathbf{J}\boldsymbol{\omega}\times\boldsymbol{\omega} + \boldsymbol{\tau}_{\mathrm{tot}}, \tag{20}$$

where $\mathbf{J}$ is the spacecraft's inertia tensor, $\boldsymbol{\omega}$ is the angular velocity vector in the spacecraft's body frame and $\boldsymbol{\tau}_{\mathrm{tot}}$ is the sum of the control and disturbance torques acting on the spacecraft also in the body frame. This is known as Euler's equation for rigid body dynamics.

Separating the total torque, $\boldsymbol{\tau}_{\mathrm{tot}}$, into the gravity gradient torque, $\boldsymbol{\tau}_{\mathrm{gg}}$, aerodynamic disturbance torque, $\boldsymbol{\tau}_{\mathrm{aero}}$, and control torques $\boldsymbol{\tau}_{\mathrm{b-dot}}$ and $\boldsymbol{\tau}_{\mathrm{align}}$, we can write (20) as

$$\mathbf{J}\dot{\boldsymbol{\omega}} = \mathrm{J}\boldsymbol{\omega}\times\boldsymbol{\omega} + \left(\boldsymbol{\tau}_{\mathrm{gg}} + \boldsymbol{\tau}_{\mathrm{aero}} + \boldsymbol{\tau}_{\mathrm{b-dot}} + \boldsymbol{\tau}_{\mathrm{align}}\right) \tag{21}$$

2.5.2 Magnetic Torque Coil Control Torque

When a long conductor is wound into a coil that a current runs through, a magnetic field is created. In the presence of an external magnetic field such as that of the Earth, the two fields interact and a moment, $\boldsymbol{\tau}_{\mathrm{M}}^{\mathrm{B}}$, is generated,

$$\boldsymbol{\tau}_{\mathrm{M}}^{\mathrm{B}} = \mathbf{v}_{\mathrm{M}}^{\mathrm{B}}\times\mathbf{m}, \tag{22}$$

where $\mathbf{v}_{\mathrm{M}}^{\mathrm{B}}$ is the local magnetic field vector in the body frame and $\mathbf{m}$ is the magnetic moment vector in the body frame generated by the set of magnetic torque coils. This magnetic field is proportional to the number of turns of the coil, N, the mean cross-sectional area of the coil, and the current through the coil, I. The constant of proportionality is the equivalent area, A, of the coil. If the area from one turn to the next is constant, then the equivalent area would just be the sum of the area of all the turns. That is

$$\mathbf{m_i} = \sum_{\mathrm{i}=0}^{\mathrm{n}} \mathrm{IA_i} = \mathrm{IA_i}\sum_{\mathrm{i}=0}^{\mathrm{n}} 1 = \mathrm{IA}(\mathrm{n}+1)\hat{\mathbf{n}}_{\mathrm{i}}.$$

With a coil of rectangular cross-section with a length, l_0 and width, w_0,

$$\mathbf{m_i} = IA(n+1)\hat{\mathbf{n}} = I(l_0 w_0)(n+1)\hat{\mathbf{n}}_i.$$

However, with a varying area, such as that of a planer spiraling coil it is difficult to intuitively determine the equivalent area.

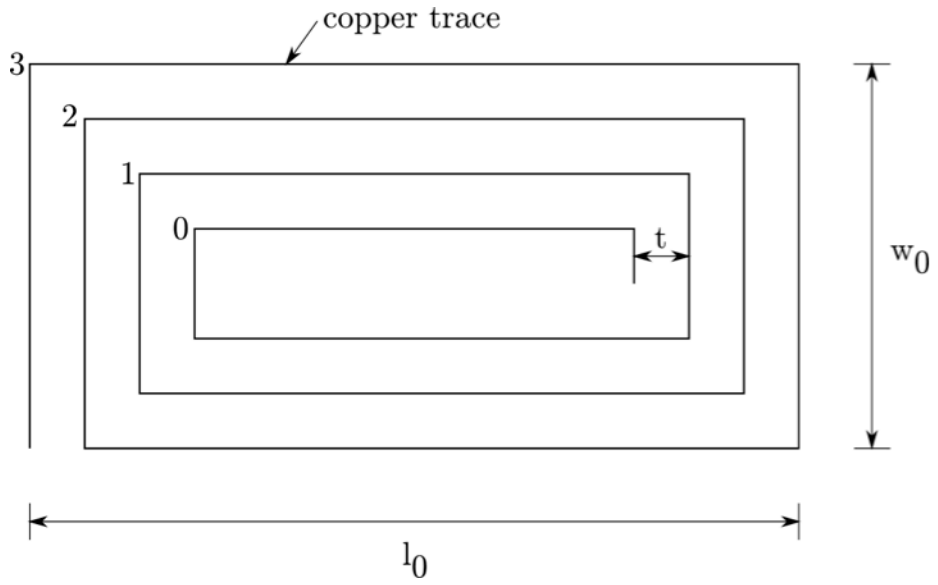

Figure 11: An idealization of magnetic torque coil.

We begin by first forming the magnetic moment in its most general form, as a sum of coils with differing areas,

$$\mathbf{m} = \sum_{i=0}^{n} IA_i\hat{\mathbf{n}}_i = I\hat{\mathbf{n}}_i \sum_{i=0}^{n} A_i,$$

where I is the current through the coil, n is one less the number of coils making up a single air-core magnetic torque coil and A_i is the area of the ith coil and $\hat{\mathbf{n}}_i$ is the normal vector to the coil in the body frame.

The planer coil is approximated as a set of rectangular loops each laying within each other (Fig. 11). The area A_i of each coil decreases with wrap count, n, since

the coil is in a plane and is spiraling inward. Assuming that the distance between each wrap, t, is constant, we have

$$\sum_{i=0}^{n} A_i = \sum_{i=0}^{n} (l_0 - 2it)(w_0 - 2it) = \sum_{i=0}^{n} l_0 w_0 - 2it(l_0 + w_0) + 4i^2 t^2$$

$$= \sum_{i=0}^{n} l_0 w_0 - (2t)(l_0 + w_0) \sum_{i=0}^{n} i + 4t^2 \sum_{i=0}^{n} i^2 .$$

Simplifying the summations of the polynomials, we get

$$\sum_{i=0}^{n} A_i = \sum_{i=0}^{n} l_0 w_0 - (2t)(l_0 + w_0) \sum_{i=0}^{n} i + 4t^2 \sum_{i=0}^{n} i^2$$

$$= l_0 w_0 (n+1) - (2t)(l_0 + w_0) \left[\frac{n(n+1)}{2}\right] + 4t^2 \left[\frac{n(n+1)(2n+1)}{6}\right].$$

Since the coil is simply just a long resistor and assuming that the driving frequency is low enough, such that the complex component of the resistance is small, the current through the coil is just $\frac{V}{R}$ where V is the voltage across the coil and R is the resistance of the coil. Therefore, the instantaneous magnetic moment, **m** of the magnetic torque coil for the ith face is

$$\mathbf{m}_i = \hat{\mathbf{n}}_i \frac{V}{R} \left\{ l_0 w_0 (n+1) - (2t)(l_0 + w_0) \left[\frac{n(n+1)}{2}\right] + 4t^2 \left[\frac{n(n+1)(2n+1)}{6}\right] \right\}. \quad (23)$$

Using (22), the magnetic moment calculated using (23) is used to compute the torque provided by H2's x-axis and y-axis magnetic torque coils.

2.5.3 Gravity-Gradient Torque

The gravity field is not uniform over a spacecraft in orbit. A part of the spacecraft closer to the Earth will experience a slightly stronger attractive force than a part that is farther from the Earth. In fact if a spacecraft is sufficiently large, there can be significant differences in gravitational force at different parts of the spacecraft

and thus a considerable torque due to the gradient in the gravity field can be created.

In our case, we exploit this torque to help the satellite stabilize in the nadir direction. The gravity gradient difference in gravitational force creates a moment, called the gravity gradient torque,

$$\boldsymbol{\tau}_{\mathrm{G}}^{\mathrm{B}} = 3\omega_0^2\left(\hat{\mathbf{v}}_{\mathrm{P}}^{\mathrm{B}} \times \mathbf{J}\hat{\mathbf{v}}_{\mathrm{P}}^{\mathrm{B}}\right), \tag{24}$$

where $\hat{\mathbf{v}}_{\mathrm{P}}^{\mathrm{B}}$ is the satellite position unit vector in the body frame, **J** is the inertia tensor, and orbit angular velocity also known as the mean motion of the orbit,

$$\omega_0 = \sqrt{\frac{\mu}{\mathrm{r}_0^3}}, \tag{25}$$

where $\mu = 3.986004415 \times 10^5 \frac{\mathrm{km}^3}{\mathrm{s}^2}$ is the Earth's gravitational parameter, and $\mathrm{r}_0$is the spacecraft's orbit radius [5].

2.5.4 Equilibria for Gravity-Gradient Stabilization

To find the equilibria for gravity gradient stabilization, we begin by setting the body angular velocity and accelerations to zero in the satellite's dynamics found in (20) as we are assuming steady state. Also we assume that there are no other dominant torques other than the gravity gradient torque. So,

$$\mathbf{0} = \mathbf{J}\dot{\boldsymbol{\omega}} + \boldsymbol{\omega} \times \mathbf{J}\boldsymbol{\omega} = 3\omega_0^2\left(\hat{\mathbf{v}}_{\mathrm{P}}^{\mathrm{B}} \times \mathbf{J}\hat{\mathbf{v}}_{\mathrm{P}}^{\mathrm{B}}\right)$$

Simplifying, we get

$$\mathbf{0} = \left(\hat{\mathbf{v}}_{\mathrm{P}}^{\mathrm{B}} \times \mathrm{J}\hat{\mathbf{v}}_{\mathrm{P}}^{\mathrm{B}}\right). \tag{26}$$

If we recall that $\hat{\mathbf{v}}_{\mathrm{P}}^{\mathrm{B}}$ as $\mathbf{R}_{\mathrm{B}}^{\mathrm{L}\,\mathrm{T}}(-\mathbf{e_3})$, it is easy to see that the cross product is zero when the position vector lines up with the third body axis. So if we let $\mathrm{a} = \hat{\mathbf{v}}_{\mathrm{P}}^{\mathrm{B}} = -\mathbf{R}_{\mathrm{B}}^{\mathrm{L}\,\mathrm{T}}\mathbf{e_3}$ then (26) simplifies to $\mathbf{a} \times \mathbf{J}\mathbf{a} = 0$. If we assume that the satellite inertial tensor is defined to its principle axes, we have

$$\mathbf{a} = \begin{bmatrix} a_1 \\ a_2 \\ a_3 \end{bmatrix} \text{ and } \mathbf{J} = \begin{bmatrix} J_{11} & 0 & 0 \\ 0 & J_{22} & 0 \\ 0 & 0 & J_{33} \end{bmatrix}.$$

Performing the cross product, we get

$$\begin{bmatrix} (J_{33} - J_{22})a_2a_3 \\ (J_{11} - J_{33})a_1a_3 \\ (J_{22} - J_{11})a_1a_2 \end{bmatrix} = \begin{bmatrix} 0 \\ 0 \\ 0 \end{bmatrix}.$$

We are assuming that the satellite is not a cylinder or a sphere of uniform mass distribution. So we know that $J_{33} - J_{22} \neq 0$, $J_{33} - J_{22} \neq 0$, and $J_{22} - J_{11} \neq 0$ and we arrive at the following system of equations:

$$\begin{bmatrix} a_2a_3 \\ a_1a_3 \\ a_1a_2 \end{bmatrix} = \begin{bmatrix} 0 \\ 0 \\ 0 \end{bmatrix}. \tag{27}$$

Recalling that $\hat{\mathbf{v}}_P^B$ is a unit vector with magnitude 1, we have the additional constraint that $a_1^2 + a_2^2 + a_3^2 = 1$. With this constraint, we can find all possible solutions to (27) (Table 1).

Table 3: Possible unit vector directions for gravity gradient stabilization.

Combined	Constrained Variables	Resulting Vector
$a_2 = 0\, a_3 = 0$	$a_1 = \pm 1$	$a = [\pm 1 \quad 0 \quad 0]^T$
$a_2 \neq 0\, a_3 = 0$	$a_1 = 0\, a_2 = \pm 1$	$a = [0 \quad \pm 1 \quad 0]^T$
$a_2 = 0\, a_3 \neq 0$	$a_1 = 0\, a_3 = \pm 1$	$a = [0 \quad 0 \quad \pm 1]^T$
$a_1 = 0\, a_3 = 0$	$a_2 = \pm 1$	$a = [0 \quad \pm 1 \quad 0]^T$
$a_1 \neq 0\, a_3 = 0$	$a_2 = 0\, a_1 = \pm 1$	$a = [\pm 1 \quad 0 \quad 0]^T$
$a_1 = 0\, a_3 \neq 0$	$a_2 = 0\, a_3 = \pm 1$	$a = [0 \quad 0 \quad \pm 1]^T$
$a_1 = 0\, a_2 = 0$	$a_3 = \pm 1$	$a = [0 \quad 0 \quad \pm 1]^T$
$a_1 \neq 0\, a_2 = 0$	$a_3 = 0\, a_1 = \pm 1$	$a = [\pm 1 \quad 0 \quad 0]^T$
$a_1 = 0\, a_2 \neq 0$	$a_3 = 0\, a_2 = \pm 1$	$a = [0 \quad \pm 1 \quad 0]^T$

Combining duplicates, there are six directions in the LVLH frame in which the satellite will assume a zero gravity gradient torque. The largest set of possible pointing directions in which the satellite can assume to ensure that there is no gravity gradient torque is

$$\mathbf{a} = \left\{ \begin{bmatrix} \pm 1 \\ 0 \\ 0 \end{bmatrix}, \begin{bmatrix} 0 \\ \pm 1 \\ 0 \end{bmatrix}, \begin{bmatrix} 0 \\ 0 \\ \pm 1 \end{bmatrix} \right\}. \tag{28}$$

These six directions are when the gravity gradient torque is zero. However, to assume that the satellite will assume these directions depends on the stability of these directions. To do this, we will need to take a look at the gravitational potential energy of the satellite assuming these pointing directions. We note that the gravitational potential energy is

$$\mathrm{E_{pot}} = \frac{3}{2}\omega_0^2\left(\mathrm{J}\hat{\mathbf{v}}_{\mathrm{P}}^{\mathrm{B}} \cdot \hat{\mathbf{v}}_{\mathrm{P}}^{\mathrm{B}}\right). \tag{29}$$

Recalling that we let $\mathbf{a} = \hat{\mathbf{v}}_{\mathrm{P}}^{\mathrm{B}}$, we see that

$$\mathrm{E_{pot}} = \frac{3}{2}\omega_0^2(\mathrm{J}\mathbf{a} \cdot \mathbf{a}) = \frac{3}{2}\omega_0^2(\mathrm{J}_{11}\mathrm{a}_1^2 + \mathrm{J}_{22}\mathrm{a}_2^2 + \mathrm{J}_{33}\mathrm{a}_3^2).$$

Following convention, the elements in H2's inertia tensor are such that $\mathrm{J}_{11} > \mathrm{J}_{22} > \mathrm{J}_{33}$. By substituting, from (28), the largest set of pointing directions for the satellite that make the gravity gradient torque zero, we see that

$$\min\{\mathrm{E_{pot}}\} = \min\left\{\frac{3}{2}\omega_0^2\mathrm{J}_{11}, \frac{3}{2}\omega_0^2\mathrm{J}_{22}, \frac{3}{2}\omega_0^2\mathrm{J}_{33}\right\} = \frac{3}{2}\omega_0^2\mathrm{J}_{33}.$$

We are looking for the minimum energy since it is only the minimum energy state in which the satellite will assume as time goes to infinity.

From this, one can conclude that the $\begin{bmatrix} \pm 1 \\ 0 \\ 0 \end{bmatrix}$ and $\begin{bmatrix} 0 \\ \pm 1 \\ 0 \end{bmatrix}$ pointing directions in the LVLH frame are max and saddle equilibria points such that if setting in these pointing directions, a small disturbance such as that created by a small amount of air drag will cause the satellite to point in either of the $\begin{bmatrix} 0 \\ 0 \\ \pm 1 \end{bmatrix}$ pointing directions. This means that the only stable equilibria for the H2 are the nadir and anti-nadir

orientations. However, there is an equal chance that H2 will point in the nadir direction compared to the anti-nadir direction. For a satellite with directional antennas, this is critical point to make as an anti-nadir pointing direction of the antenna may create a condition where the satellite will not be able to close the transponder's link budget with the radar stations. Therefore it is critical that the boom deployment be at the right time. How this dilemma is handled will be discussed later.

2.5.5 Aerodynamic Torque

For spacecraft in Low Earth Orbit (LEO), there is enough atmosphere such that the aerodynamic torque is not negligible. Generally, the center of pressure of a face on the satellite does not line up with the center of mass for the spacecraft and therefore imparting an aerodynamic torque on the spacecraft. According to [9], this torque can be modeled as

$$\boldsymbol{\tau}_{\text{aero}} = -\frac{1}{2}\frac{\rho(\text{h})}{\text{m}}|\mathbf{v}_{\text{rel}}|^2 \sum_{\text{i}=1}^{\text{n}} \gamma_{\text{i}} \text{A}_{\text{i}} \text{C}_{\text{D,i}} (\hat{\mathbf{n}}_{\text{i}} \cdot \hat{\mathbf{v}}_{\text{rel}})^2 \left(\hat{\mathbf{v}}_{\text{rel}} \times \mathbf{r}_{\text{cp,i}}\right), \tag{30}$$

where $\rho(\text{h})$ is the air density at altitude h, m is the mass of the spacecraft, $\mathbf{v}_{\text{rel}}$ is the relative velocity vector represented in the spacecraft body frame, A_{i} is the cross-sectional area of face i measured normal to the face, $\text{C}_{\text{D,i}}$ is the coefficient of drag for face i, $\hat{\text{n}}_{\text{i}}$ is the unit vector normal to face i, $\hat{\mathbf{v}}_{\text{rel}}$ is the relative velocity unit vector, $\mathbf{r}_{\text{cp,i}}$ is the vector from the center of mass to the center of pressure on face I and γ_i is a binary operator which determines if a face is currently being impeded by the atmosphere and is defined as

$$\gamma_{\text{i}} = \begin{cases} 1 & \hat{\mathbf{n}}_{\text{i}} \cdot \hat{\mathbf{v}}_{\text{rel}} > 0 \\ 0 & \text{otherwise} \end{cases}.$$

It is assumed that the atmosphere has the same rotation velocity of the Earth so $\mathbf{v}_{rel}$ is defined as

$$\mathbf{v}_{\text{rel}} = \dot{\mathbf{v}}_{\mathbf{P}}^{\mathbf{E}} - \boldsymbol{\omega}_{\oplus} \times \mathbf{v}_{\mathbf{P}}^{\mathbf{E}},$$

where $\dot{\mathbf{v}}_{\mathbf{P}}^{\mathbf{E}}$ and $\mathbf{v}_{\mathbf{P}}^{\mathbf{E}}$ are the velocity and position of the spacecraft in ECEF coordinates and $\boldsymbol{\omega}_{\oplus}$ is the angular rotational velocity vector of Earth.

To determine the air density at the altitude of the spacecraft, ρ, the exponential atmosphere model was used. This is a very simple approach and has moderate accuracy for general studies. The model is

$$\rho(h) = \rho_0 \exp\left(-\frac{h - h_0}{H}\right),$$

where h_0, is the reference altitude, ρ_0, the reference density, and H is the scale height and must be obtained from a lookup table. For 500 km altitude, h_0=500 km, $\rho_0 = 6.967\times10^{-13}\,\frac{kg}{m^3}$, and $H = 63.822\ km$. So the density at 500 km altitude is approximately $6.967\times10^{-13}\,\frac{kg}{m^3}$. To put this into perspective, the density of the atmosphere at sea level is $1.225\,\frac{kg}{m^3}$ so the density of air at 500 km is less than one part per trillion than that on Earth.

2.5.6 Center of Pressure Calculation

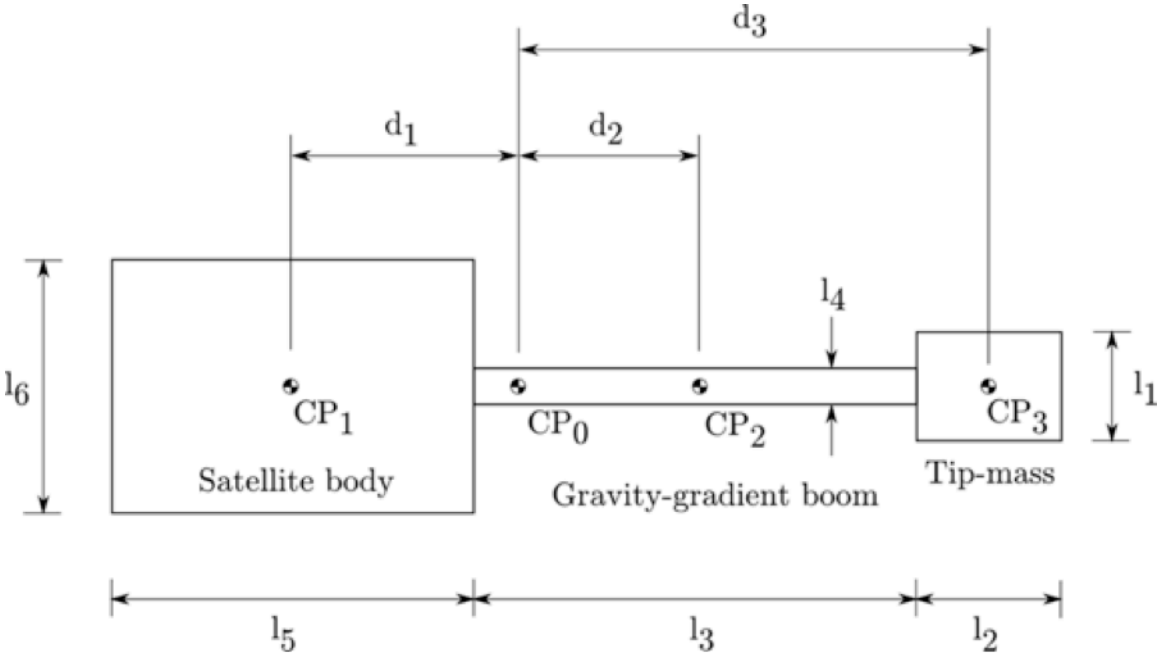

Figure 12: The simplified center of pressure model and distance variables for H2.

To solve for the location of the center of pressure on each face of the satellite, we first break the broadside area into components of simpler shapes (Fig. 12). The center of pressure for each simple shape is at the centroid of the shape. Then, a moment about the center of pressure for the broadside of the satellite is calculated

$$+\mathrm{CW}\sum \mathrm{M}_0 = 0; \mathrm{F}_2\mathrm{x}_2 + \mathrm{F}_3\,\mathrm{x}_3 - \mathrm{F}_1\mathrm{x}_1 = 0.$$

The two other constraint equations are

$$\mathrm{d}_1 + \mathrm{d}_2 = \frac{\mathrm{l}_5}{2} + \frac{\mathrm{l}_3}{2}$$

and

$$\mathrm{d}_1 + \mathrm{d}_2 + \mathrm{d}_3 = \frac{\mathrm{l}_2}{2} + \mathrm{l}_3 + \frac{\mathrm{l}_5}{2}.$$

Putting this into linear algebra form we have

$$\mathrm{C} = \mathrm{Ax} = \begin{bmatrix} -\mathrm{F}_1 & \mathrm{F}_2 & \mathrm{F}_3 \\ 1 & 1 & 0 \\ 1 & 0 & 1 \end{bmatrix} \begin{bmatrix} \mathrm{d}_1 \\ \mathrm{d}_2 \\ \mathrm{d}_3 \end{bmatrix} = \begin{bmatrix} 0 \\ \frac{\mathrm{l}_5}{2} + \frac{\mathrm{l}_3}{2} \\ \frac{\mathrm{l}_2}{2} + \mathrm{l}_3 + \frac{\mathrm{l}_5}{2} \end{bmatrix}.$$

Solving for A^{-1}, we get that

$$\mathrm{x} = \mathrm{A}^{-1}\mathrm{C} = \frac{1}{\mathrm{F}_1 + \mathrm{F}_2 + 2\mathrm{F}_3} \begin{bmatrix} -1 & \mathrm{F}_2 + \mathrm{F}_3 & \mathrm{F}_3 \\ 1 & \mathrm{F}_1 + \mathrm{F}_3 & \mathrm{F}_3 \\ 1 & -(\mathrm{F}_1 + \mathrm{F}_3) & \mathrm{F}_1 + \mathrm{F}_2 + \mathrm{F}_3 \end{bmatrix} \begin{bmatrix} 0 \\ \frac{\mathrm{l}_5}{2} + \frac{\mathrm{l}_3}{2} \\ \frac{\mathrm{l}_2}{2} + \mathrm{l}_3 + \frac{\mathrm{l}_5}{2} \end{bmatrix}.$$

Here the drag forces on each of the faces $\mathrm{F}_1, \mathrm{F}_2, \mathrm{F}_3$ are

$$\mathrm{F}_1 = \frac{1}{2}\rho(\mathrm{h})\mathrm{C}_\mathrm{d}(\mathrm{l}_6\mathrm{l}_5)|\mathbf{v_{rel}}|^2$$

$$\mathrm{F}_2 = \frac{1}{2}\rho(\mathrm{h})\mathrm{C}_\mathrm{d}(\mathrm{l}_4\mathrm{l}_3)|\mathbf{v_{rel}}|^2$$

$$\mathrm{F}_3 = \frac{1}{2}\rho(\mathrm{h})\mathrm{C}_\mathrm{d}(\mathrm{l}_2\mathrm{l}_1)|\mathbf{v_{rel}}|^2.$$

For the simplified geometry illustrated in Figure 12, the location of the center of pressure for all x- and y-axis faces were considered identical. The coefficient of drag is recommended by Vallado to be set to 2.2 [9].

2.6 ADCS Mode Control Laws

Inspiration for the design of ADCS system was drawn from the simplicity of the early TRANSIT satellite system developed in the 1960s [16]. Although gravity-gradient stabilization is a pastime today with the birth of nonlinear active control schemes, gravity-gradient stability was a new concept put to practice more than 50 years ago. Thus, the methods developed to achieve gravity gradient stabilization were intuitive and simple. It is this simplicity that made following the designs of early satellites such as the TRANSIT system, attractive to duplicate for H2.

2.6.1 Detumbling Control Law

The body rotation rates for a tumbling satellite just inserted into orbit are usually far greater than the rotation rate of the local magnetic field vector passing through the satellite. Especially for CubeSats that are usually regarded as secondary payloads, little care is paid to the tip-off rates imparted on a CubeSat upon insertion. Since the magnetic field direction and magnitude varies slowly compared to the tumbling motion of the satellite, the magnetic field can be used as a reference vector for detumbling. For detumbling, H2 used a simple control law called the B-Dot law. There are two versions of this law: one is a proportional controller (31) while the other is a bang-bang controller (33). We will go over the proportional control version of the law first.

2.6.2 Proportional Detumbling Control Law

As proposed in [17], the proportional detumbling control law has the form

$$\mathbf{m_{bdot}} = -k\dot{\mathbf{v}}_M^B, \tag{31}$$

where $\dot{\mathbf{v}}_{\mathrm{M}}^{\mathrm{B}}$ is the rate of change of the measured magnetic field in the spacecraft body frame and k is a scalar gain value for the torque. Theoretically, k can be any positive number and the satellite can then detumble arbitrarily fast. However, in reality the value of k must be constrained to account for magnetic torque coil saturation. If the desired torque cannot be provided by the set of magnetic torque coils, then the scalar must be reduced so that even the weakest magnetic torque coil is accounted for.

To do this, we first preserve the controller's desired direction. Normalizing the magnetic moment that would produce the desired torque,

$$\widehat{\mathbf{m}}_{\mathbf{d}} = \frac{\mathbf{m_d}}{|\mathbf{m_d}|}.$$

We then define a vector

$$\mathbf{c} = \begin{bmatrix} \mathrm{m}_{\mathrm{x,max}} |\widehat{\mathrm{m}}_1|^{-1} \\ \mathrm{m}_{\mathrm{y,max}} |\widehat{\mathrm{m}}_2|^{-1} \\ \mathrm{m}_{\mathrm{z,max}} |\widehat{\mathrm{m}}_3|^{-1} \end{bmatrix},$$

where $\mathrm{m}_{\mathrm{i,max}}$ is the maximum magnetic moment that can be produced by the ith-axis magnetic torque coil. Taking the minimum value of $\mathbf{c}$ accounts for even the weakest magnetic torque coil and identifies the scalar value that when multiplied to $\widehat{\mathbf{M}}_{\mathbf{d}}$ will produce a torque that is in the same direction as what is desired when applying the maximum magnetic moment to the weakest coil. The applied magnetic moment is then

$$\mathbf{m_{app}} = \min(\mathbf{c})\widehat{\mathbf{m}}_{\mathbf{d}} \tag{32}$$

Then using (22), the control torque is produced.

2.6.3 Bang-Bang Detumbling Control Law

For the bang-bang control law there is no need to do any calculations to rescale the gain for actuator saturation [17]. Instead, the following logic is used

$$\mathbf{m_{bdot}} = \begin{bmatrix} -m_{1,max}\,sgn(\dot{B}_x) \\ -m_{2max}\,sgn(\dot{B}_y) \\ -m_{3,max}\,sgn(\dot{B}_z) \end{bmatrix}. \tag{33}$$

An advantage of the bang-bang detumbling controller allows for the control electronics to be simpler since the PWM generation is no longer necessary. Theoretically, the same set of magnetic torque coils, the bang-bang controller should dissipate the satellite's kinetic energy faster than the proportional controller [17].

2.6.4 Alignment Mode Control Law

For a satellite to align itself with the magnetic field, it must constantly generate a restoring magnetic torque. However, when doing so, without the presence of damping, the spacecraft will oscillate about the minimum energy equilibrium point. We want the satellite's magnetic field vector to track the magnetic field of the Earth. To describe this rigorously, we want the rate of change of the magnetic field in the satellite's body frame to approach zero and we want H2 to point along the magnetic field. To come up with the alignment mode control law, we summed two terms together that would ensure the pointing requirement and the rate requirement. Similar to the control investigated in [18], the control torque during the alignment mode is

$$\mathbf{m_{align}} = -k\dot{\mathbf{v}}_M^B + \frac{I_{z,max}}{2}(l_0 w_0) n \mathbf{b_3}, \tag{34}$$

where n is the number of wraps, l_0 is the length of the coil, w_0 is the width, and $\mathbf{b_3}$ is the third body direction in the body frame. The bias magnetic moment continually attempts to align the satellite with the magnetic field and $-k\dot{\mathbf{v}}_M^B$ is the damping term. Like the B-Dot controller, the actuator constraints must be considered. We normalize the magnetic moment that would produce the desired torque,

$$\hat{\mathbf{m}}_\mathbf{d} = \frac{\mathbf{m_d}}{|\mathbf{m_d}|}.$$

We then define a vector

$$\mathbf{c} = \begin{bmatrix} m_{1,max}|\hat{m}_1|^{-1} \\ m_{2,max}|\hat{m}_2|^{-1} \\ m_{3,max}|\hat{m}_3|^{-1} \end{bmatrix}.$$

The applied magnetic moment is then

$$\mathbf{m_{app}} = \min(\mathbf{c})\hat{\mathbf{m}}_\mathbf{d}.$$

Then using (22), the control torque is produced.

Chapter 3
Hardware Implementation & Operation

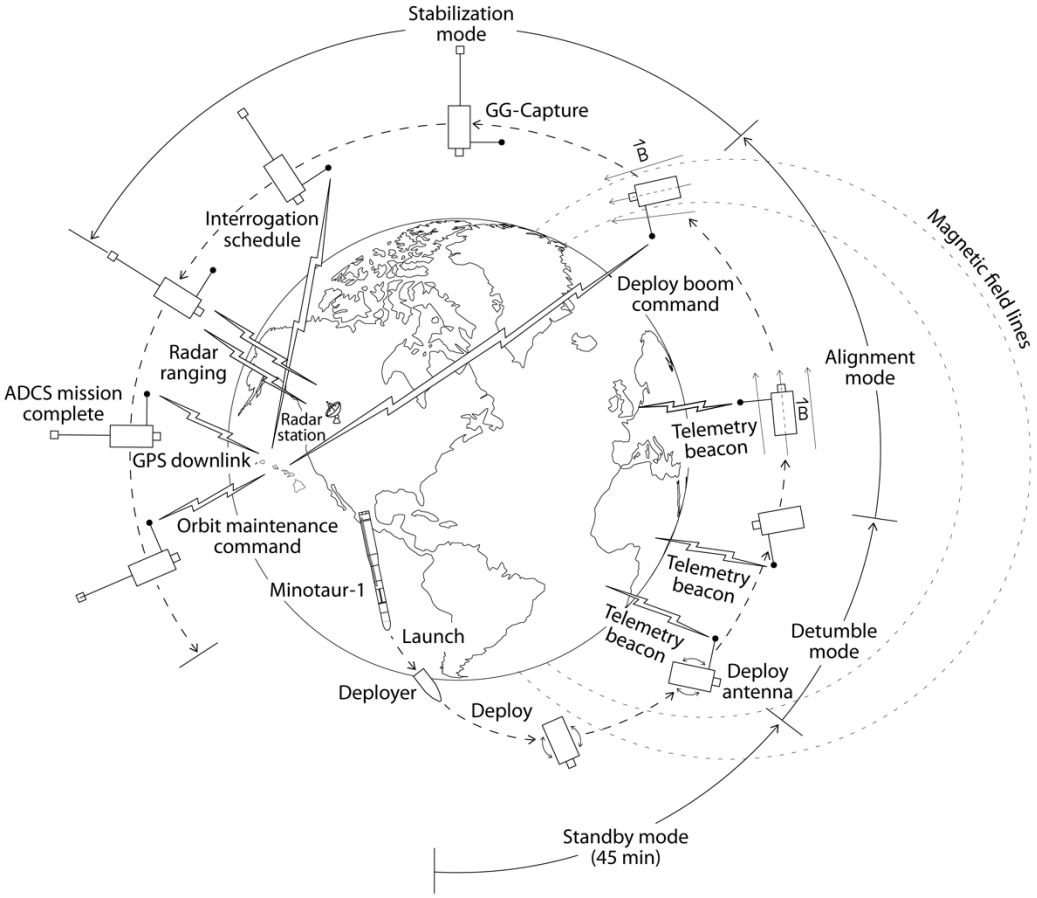

Figure 13: H2's orbit modes.

3.1 ADCS Modes of Operations

H2 is at an orbit of 500 km altitude with an inclination of 40.5 degrees. As summarized in Figure 13, upon entering orbit, there is a 45-minute waiting period in which H2 remains powered off after which it will power up and deploy its communications antenna. After antenna deployment, H2 begins beaconing health information every 15 seconds while attempting to detumble. After orbit

insertion, H2 can be tumbling at a rate of up to 10 degrees/sec/axis. At this point the satellite actively detumbles to a slower tumble rate and enters alignment mode. In the alignment mode, H2 locks onto the Earth's magnetic field until commanded by the ground station to enter the final phase of achieving nadir pointing, stabilization. The attitude determination algorithm recommends to the ground station when it estimates that H2 is close enough to the local vertical direction for nadir pointing. In the stabilization mode the gravity-gradient boom is deployed in a controlled fashion while H2 dampens oscillations using its magnetic torque coils using the detumbling law. After the boom has been completely deployed, H2 will remain stabilized in the nadir direction indefinitely until the aerodynamic drag acting on it brings H2 back to Earth.

3.1.1 ADCS System Description

H2's ADCS uses a magnetometer, a set of photodiodes, and a set of IR sensors to determine its attitude. H2 controls its attitude using its gravity gradient boom and three magnetic torque coils (Fig. 14).

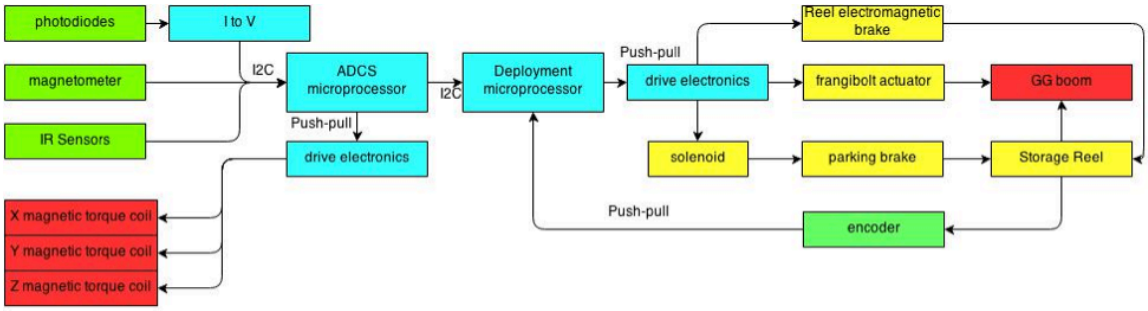

Figure 14: H2's ADCS hardware diagram.

3.1.1.1 Gravity-Gradient Boom Deployer

A trade study was performed relating boom length to steady state error due to aerodynamic drag and it was determined that the boom must be at least 5 m long to meet the steady-state error requirement. In addition, testing determined that the boom must deploy in a controlled fashion. This is because the boom material has failed during uncontrolled deployments when the reel abruptly stops. at the

end of the deployment. Lastly, the tip-mass for the boom was to be secured to the satellite structure using a Frangibolt® hold-release mechanism for the gravity-gradient boom deployer to survive launch loads.

The gravity gradient deployer can be separated into several major groups: storage reel, electromagnetic brake, parking brake, compensator, tip-mass, Frangibolt ® hold-release mechanism, boom, and control electronics (Fig. 15).

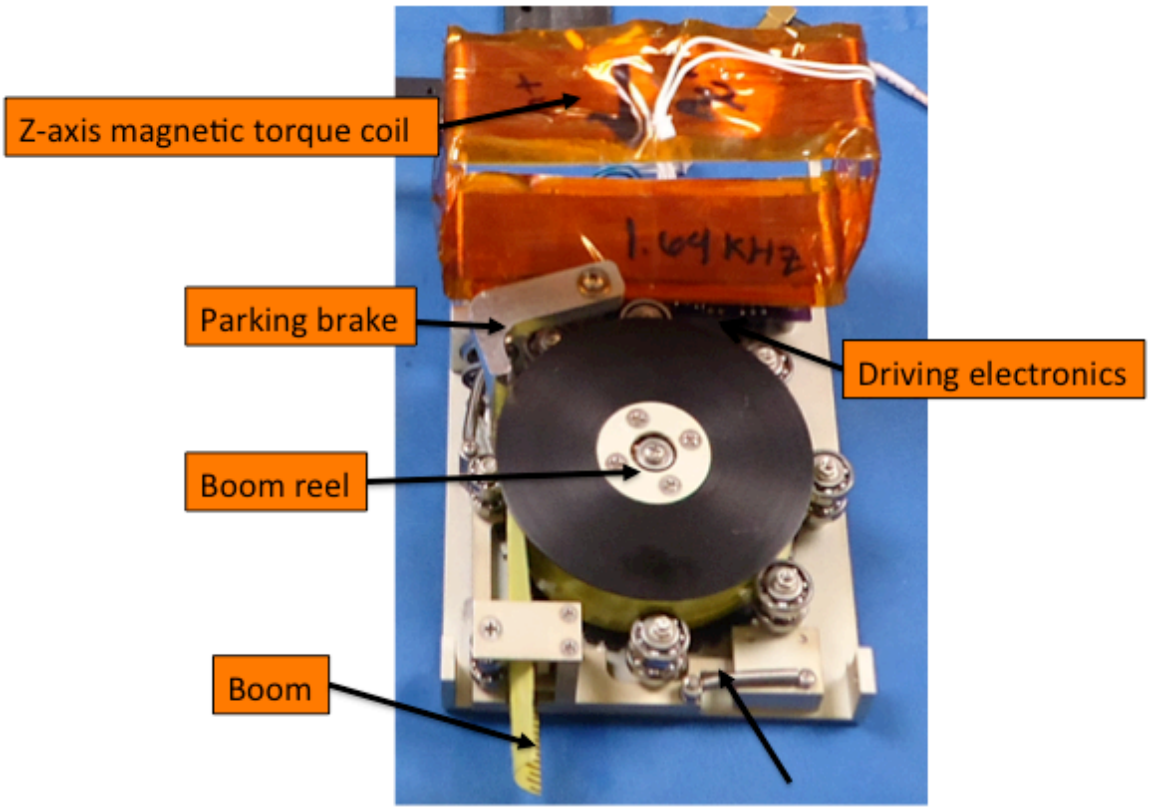

Figure 15: H2's GG boom deployer.

3.1.1.2 Boom Reel

The inner surface of the reel has a flat machined onto it where the boom (tape measure) attaches via the tape clamp using #4 screws. The tape then wraps around the reel in the direction of the lead-in. The lead-in prevents excessive stresses that would cause the tape to yield if the tape is wound tightly. It has been demonstrated that the 5 m boom can comfortably be stored on the reel with

a maximum storage capacity of 8 m. Roller bearings are press fitted into the bore of the reel, which is then secured into the reel using a retaining cap. A custom-machined shaft mates with the roller bearings and fastens the reel to the ACS bracket. An encoder wheel is engraved into the anodize coating on the bottom of the reel for sensing the speed of the reel during deployment (Fig. 16).

Figure 16: The optical encoder wheel engraved on underside of boom reel.

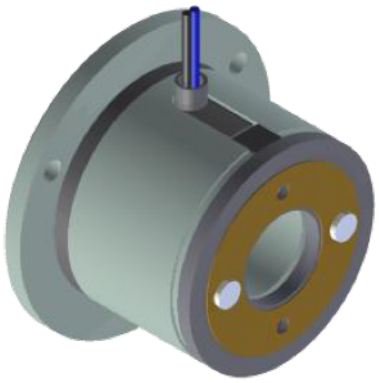

Figure 17: H2's Electromagnetic brake [20].

3.1.1.3 Electromagnetic Brake

An electromagnetic brake is used to control the deployment rate of the boom (Fig. 17). With the boom wound onto the reel, it naturally wants to unfurl, creating a torque about the reel axis and causing it to spin. For compactness, the electromagnetic brake nests inside the reel and attaches to the underside of the

reel. As mentioned before, when uncontrolled, the velocity of the reel at the end of deployment is so great that the boom itself would fail and separate from the satellite.

3.1.1.4 Parking Brake

To reduce the shear loading on the Frangibolt ® fastener, a parking brake prevents the reel from rotating during launch (Fig. 15). The parking brake also ensures that the reel does not unfurl during launch, which may cause binding when commanded to extend. The parking brake consists of a machined arm with a pin attached to the end opposite the fulcrum. The pin mates with teeth that are machined into the reel to lock it in place. A solenoid is used to actuate the parking brake.

3.1.1.5 Compensator

Due to the large change in diameter of the boom during extension, a fixed boom guide on the ACS mounting plate would mean that the boom will point off to the side at the end of the extension and would no longer be parallel to the z-axis of the satellite. To prevent this, a passive mechanism, called a compensator, was designed to slide with the decreasing diameter of the reel such that the boom length is always parallel to the z-axis throughout deployment (Fig. 15).

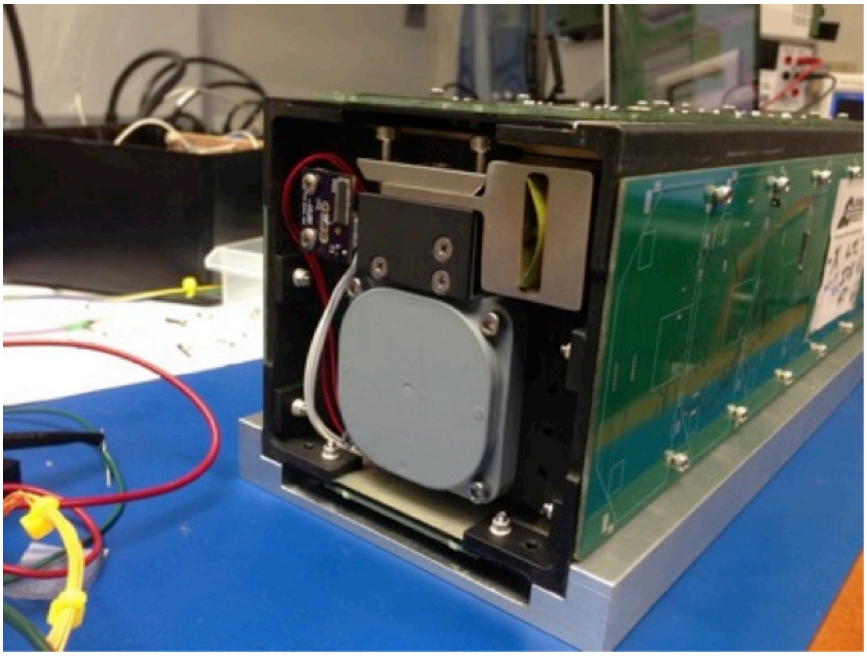

Figure 18: The Frangibolt ® Hold-Release Mechanism on H2.

3.1.1.6 Tip-mass

The tip-mass for the boom has a mass of 100 g and is made from stainless steel 304. The overall shape was waterjetted, and the clearance hole for the Frangibolt® actuator fastener and slots to clear the separation springs were milled (Fig. 18).

3.1.1.7 Frangibolt® Hold-release Mechanism

To attach the boom tip-mass securely to the structure, a COTS hold-release mechanism called a Frangibolt® actuator was used (Fig. 18). The Frangibolt® consists of an expanding SMA barrel and a titanium bolt with a weakened section. When the SMA barrel is heated by running a current through it, the barrel expands and breaks the fastener. The separating mechanism then separates the broken fastener to allow for the boom to extend unobstructed. Although the reel brake is designed to prevent the boom from extending prematurely, the Frangibolt® offers a final contingency measure that prevents the boom from extending prematurely.

3.1.1.8 Control Electronics

On the ACS bracket assembly there is a solenoid actuator for the parking brake and the electromagnetic brake. For each actuator there are driving electronics on the deployment board. The deployment board receives a command from the ADCS microprocessor to initiate the deployment process and the deployment board processor takes care of the rest (Fig. 19). This allows the ADCS deployment to occur in parallel and independent of the other satellite processes.

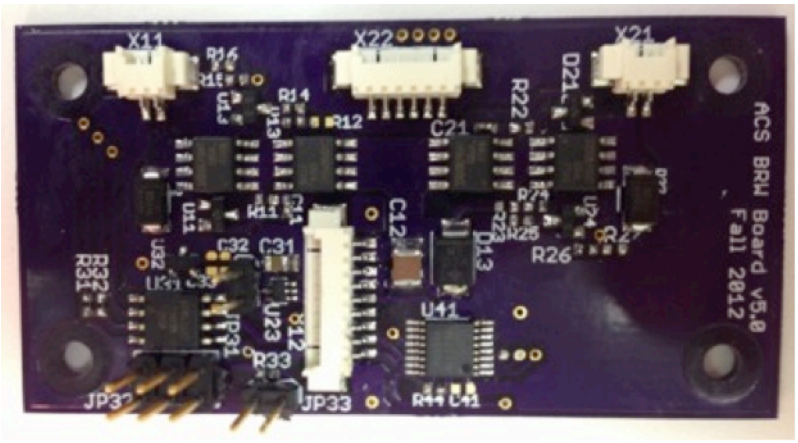

Figure 19: H2's boom deployment electronics.

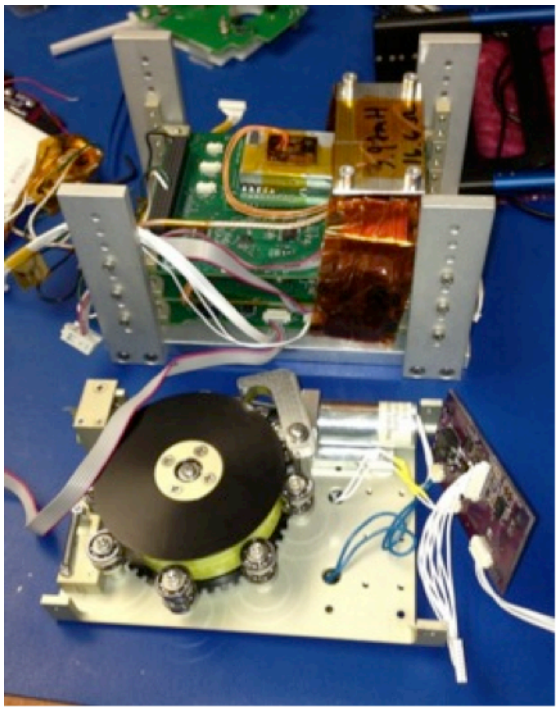

Figure 20: H2's ACS bracket before integration with CSI stack

3.1.2 Boom Buckling Moment Computation

When the satellite is spinning and deploying the gravity-gradient boom, there is the possibility that the boom could buckle due to deceleration in angular rotation of the satellite. Buckling of the boom can cause damage to the satellite's solar panels if the tip-mass collides with them. In addition, the deployment of the boom must be benign enough of an event such that the orientation for the satellite is not severally affected due to disturbance torques imparted by the extending boom. To answer these questions, a bending moment analysis was performed to calculate the bending moment on the boom during deployment and determine whether or not the boom will buckle during deployment in space.

We approximate H2 as a composite rigid body with the length of the boom as the shape variable (Fig. 21). The body of the satellite is approximated as a block of material with uniform density. The tip-mass is also assumed to have a uniform density. The boom is assumed to be a slender rod of rectangular cross-section that changes length.

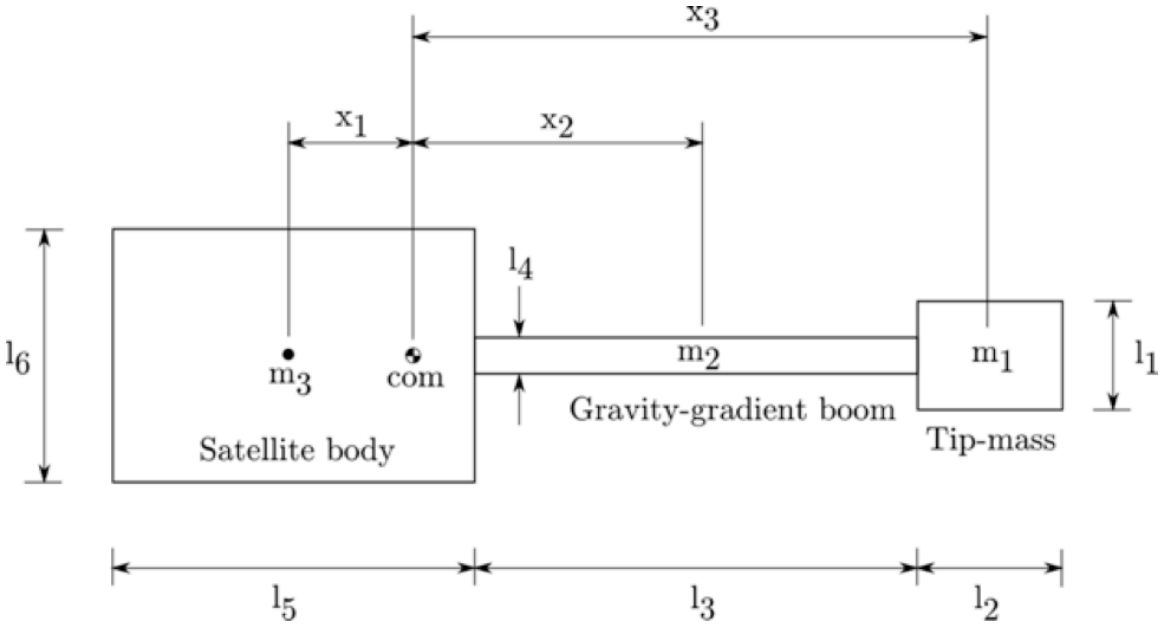

Figure 21: An approximation of H2 as composite masses.

3.1.2.1 COM Approximation

The first step is to approximate the location of the center of mass. To do this, we form the moment balance,

$$+\mathrm{CW}\sum \mathrm{M_{COM}} = 0;\ -\mathrm{m_3\,x_1} + \mathrm{m_2 x_2} + \mathrm{m_1 x_3} = 0,$$

where $\mathrm{m_1}$ is the mass of the tip-mass, $\mathrm{m_2}$ is the mass of the boom that has been extended, and $\mathrm{m_3}$ is the mass of the satellite body, $\mathrm{x_1}$ is the distance from the center of mass of the satellite body to the center of mass of the entire satellite, $\mathrm{x_2}$ is the distance of the center of mass of the boom to the center of mass of the entire satellite, and $\mathrm{x_3}$ is the distance of the center of the end mass to the center of mass of the entire satellite.

The two remaining equations that complete the three constraints are

$$\mathrm{x_1} + \mathrm{x_2} = \frac{\mathrm{l_3}}{2} + \frac{\mathrm{l_5}}{2}$$
$$\mathrm{x_1} + \mathrm{x_3} = \tfrac{\mathrm{l_2}}{2} + \tfrac{\mathrm{l_5}}{2} + \mathrm{l_3},$$

where $\mathrm{l_3}$ is the variable length of the boom, $\mathrm{l_5}$ is the length of the satellite body, and $\mathrm{l_2}$ is the length of the tip-mass.

Putting into linear algebra form, we have the following system:

$$\mathrm{C} = \mathrm{Ax} = \begin{bmatrix} 0 \\ \frac{\mathrm{l_2}}{2} + \frac{\mathrm{l_5}}{2} + \mathrm{l_3} \\ \frac{\mathrm{l_3}}{2} + \frac{\mathrm{l_5}}{2} \end{bmatrix} = \begin{bmatrix} -\mathrm{m_3} & \mathrm{m_2} & \mathrm{m_1} \\ 1 & 0 & 1 \\ 1 & 1 & 0 \end{bmatrix} \begin{bmatrix} \mathrm{x_1} \\ \mathrm{x_2} \\ \mathrm{x_3} \end{bmatrix}.$$

Solving for x, we have

$$\mathrm{x} = \mathrm{A^{-1}C} = \frac{1}{\mathrm{m_1} + \mathrm{m_2} + \mathrm{m_3}} \begin{bmatrix} -1 & \mathrm{m_1} & \mathrm{m_2} \\ 1 & -\mathrm{m_1} & \mathrm{m_1} + \mathrm{m_3} \\ 1 & \mathrm{m_2} + \mathrm{m_3} & -\mathrm{m_2} \end{bmatrix} \begin{bmatrix} 0 \\ \frac{\mathrm{l_2}}{2} + \frac{\mathrm{l_5}}{2} + \mathrm{l_3} \\ \frac{\mathrm{l_3}}{2} + \frac{\mathrm{l_5}}{2} \end{bmatrix}.$$

3.1.2.2 Moment of Inertia Approximation

As the boom is extended, the inertia of the satellite increases, causing the satellite to have a negative angular acceleration due to the conservation of angular momentum. Therefore it is important to calculate the inertia as a function of the length of the boom to determine the deceleration of the satellite.

First, the principle inertia values of each of the three components are first individually calculated. Both the satellite body and tip-mass are modeled as homogenous blocks. The moment of inertia for a general block is the following:

$$I_{xx,tipmass} = \frac{1}{12} m_1 (l_1^2 + l_2^2),$$

where l_1 is the width of the endmass and l_2 is the length. It is important to note that both of these dimensions are taken perpendicular to the spin axis of the component.

The principle inertia value of a slender rod about the same axis is

$$I_{xx,boom} = \frac{1}{12} (\rho_{boom} l_3)(l_3^2 + l_4^2),$$

where ρ_{boom} is the mass per unit length of the boom, l_3 is the length of boom and l_4 is the width of the boom.

The principle inertia value of the satellite body about its own center of mass is

$$I_{xx,body} = \frac{1}{12} m_3 (l_6^2 + l_5^2),$$

where l_5 and l_6 are the length and width of the satellite body. Using the parallel axis theorem, these principle inertia values are converted to inertia values about the COM of the satellite,

$$I_{boom,COM} = I_{xx,boom} + m_2 x_2^2$$

$$I_{body,COM} = I_{xx,body} + m_3 x_1^2$$

$$I_{tipmass,COM} = I_{xx,tipmass} + m_1 x_3^2$$

Now that all of the inertias are about the COM axis, they can be summed to arrive at the overall approximated moment of inertia for the satellite,

$$\begin{aligned} I_{tot,com} &= I_{tipmass,COM} + I_{body,COM} + I_{boom,COM} \\ &= \frac{1}{12} m_1 (l_1^2 + l_2^2) + m_1 x_3^2 + \frac{1}{12} m_3 (l_6^2 + l_5^2) + m_3 x_1^2 \\ &+ \frac{1}{12} m_2 (l_3^2 + l_4^2) + m_2 x_2^2. \end{aligned} \tag{35}$$

We solve for the radius of gyration of the satellite, boom and tip-mass composite body by taking the combined inertias of the tip-mass and boom and equating it to the inertia for a particle with a massless extension from the rotation axis,

$$\begin{aligned} I_{tipmass,COM} + I_{body,COM} + I_{boom,COM} = \\ = \frac{1}{12} m_1 (l_1^2 + l_2^2) + m_1 x_3^2 + \frac{1}{12} m_3 (l_6^2 + l_5^2) + m_3 x_1^2 \\ + \frac{1}{12} m_2 (l_3^2 + l_4^2) + m_2 x_2^2 = (m_1 + m_2 + m_3) r^2 \end{aligned}$$

Therefore solving for the radius of gyration, we arrive at

$$r(l_3, x_1, x_2, x_3) = \sqrt{\frac{\frac{1}{12} m_1 (l_1^2 + l_2^2) + m_1 x_3^2 + \frac{1}{12} m_3 (l_6^2 + l_5^2) + m_3 x_1^2 + \frac{1}{12} m_2 (l_3^2 + l_4^2) + m_2 x_2^2}{m_1 + m_2 + m_3}}$$

Although it is possible to solve for $\dot{r}$ and $\ddot{\theta}$ analytically, it is sufficient to come up with a numerical approximation in the interest of saving time. Using an Euler approximation for the derivatives while conserving angular momentum,

$$\omega_i = \frac{I_{i-1}\omega_{i-1}}{I_i}, \qquad \ddot{\theta}_\imath \approx \frac{\omega_i - \omega_{i-1}}{t_i - t_{i-1}}, \text{and } \dot{r} \approx \frac{r_i - r_{i-1}}{t_i - t_{i-1}}.$$

The tangential acceleration acting on the point mass at the end of the boom is

$$a_t = r\ddot{\theta} + 2\dot{r}\dot{\theta} \tag{36}$$

So substituting the discrete forms from above,

$$a_{t,i} = r_i\left(\frac{\omega_i - \omega_{i-1}}{t_i - t_{i-1}}\right) + 2\left(\frac{r_i - r_{i-1}}{t_i - t_{i-1}}\right)\left(\frac{I_{i-1}\omega_{i-1}}{I_i}\right). \tag{37}$$

The tangential force acting on the particle is then given by

$$F_{t,i} = (m_{tipmass} + m_{boom} + m_{body})a_t = (m_{tipmass} + m_{boom} + m_{body})(r\alpha + 2\dot{r}\omega). \tag{38}$$

The root of the appendage does not extend all the way to the axis of rotation and is at the surface of the –z face of H2. Therefore the bending moment is calculated by

$$M_b = F_t\left(x_3 - x_2 + \frac{l_3}{2}\right). \tag{39}$$

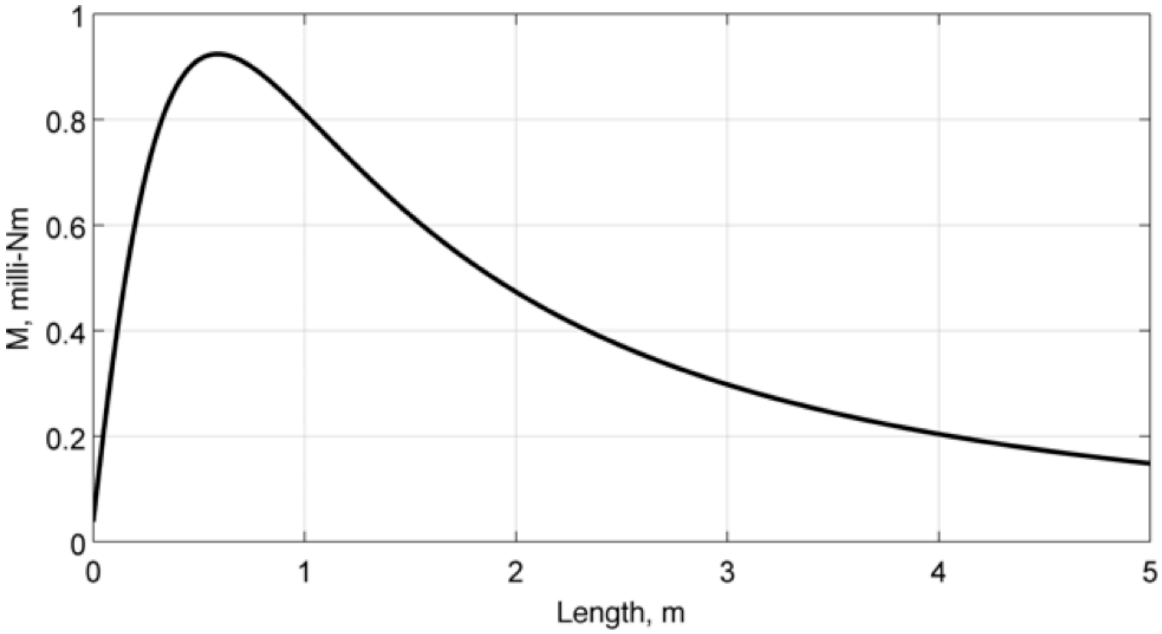

Figure 22: The simulated boom bending moment. The estimated bending moment is less than 1 mNm for a deployment rate of 60 deg/sec and a satellite spin rate of 1 deg/sec.

A simulation for calculating the bending moment was written in MATLAB while the boom deployed (Fig. 22).

The maximum bending moment of about 0.9 mN·m was simulated to occur at an extension of 0.5 m. This would be approximately 18 seconds into deployment.

To determine the minimum bending moment threshold for the boom, we extended the tape, facing concave down, upside down until the weight force of the tape itself is enough to buckle the tape (Fig. 23 and 24).

Figure 23: The tape measure blade shown just before buckling.

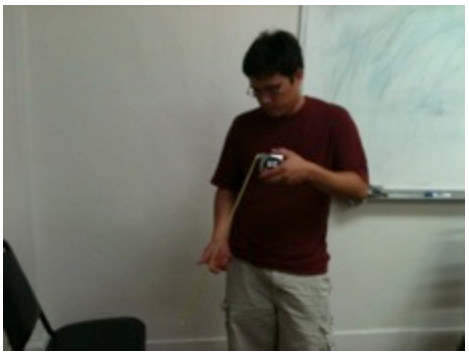

Figure 24: The tape measure blade after buckling under its own weight.

The tape measure buckled at approximately 27 in of extension. With a measured unit weight of 50 g/m for the blade, we can calculate the critical bending moment, $\mathrm{M_c}$, which caused the tape to buckle. The calculation went as follows:

$$\mathrm{M_c} = \mathrm{FL} = (27\ \mathrm{in})\left(\frac{1\ \mathrm{m}}{39.37\ \mathrm{in}}\right)\left(0.05\ \frac{\mathrm{kg}}{\mathrm{m}}\right)\left(9.81\ \frac{\mathrm{m}}{\mathrm{s^2}}\right)\left(\frac{27}{2}\ \mathrm{in}\right)\left(\frac{1\ \mathrm{m}}{39.37\ \mathrm{in}}\right)$$
$$= 0.115\ \mathrm{Nm}.$$

The minimum bending moment required to buckle the 1-inch blade is approximately 115 mN·m. Since the maximum bending moment approximated by the simulation is less than 1 mN·m at a rate of extension of 60 deg/sec, it was concluded that the boom has enough structural integrity to survive deployment in space at the beginning of stabilization mode. Therefore the disturbance torque on H2 during deployment would be the governing factor when choosing a deployment velocity.

The corresponding angular acceleration and angular velocity is shown below to show the deceleration of H2 during extension (Fig. 25).

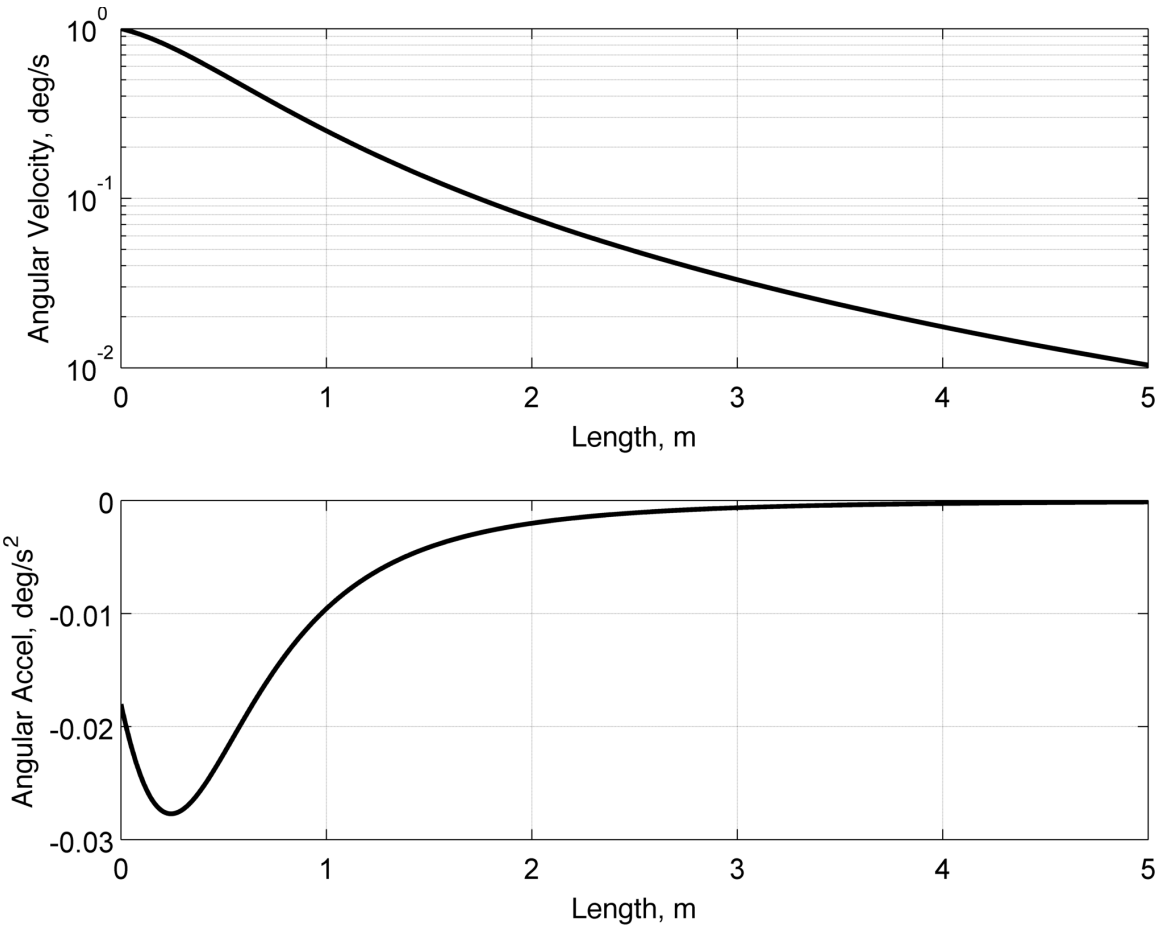

Figure 25: The angular acceleration and velocity for H2 as the boom is deployed. H2's deceleration peaks at and extension of 0.24 m.

We see that the angular acceleration is indeed negative and peaks at the same position where the maximum bending moment occurs. The angular velocity also reduces by two orders of magnitude during the extension.

3.1.3 Magnetic Torque Coils

Embedded into each of the four solar panels on H2 are 100 wraps of copper traces that create a magnetic moment. Figure 26 shows the circuit layout for one of the x-axis magnetic torque coils and associated electronics.

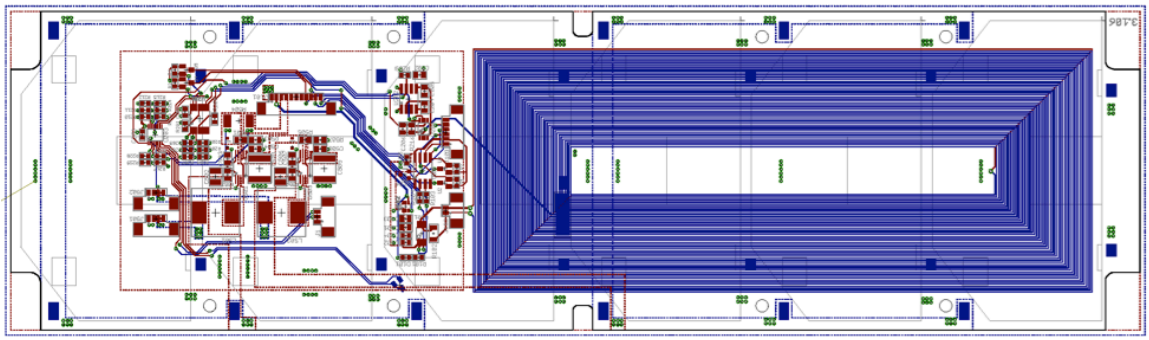

Figure 26: The Eagle® layout for x-axis magnetic torque coil.

Figure 27: Attaching the x-axis solar panel to H2 during final assembly.

Each of the x- and y-axis solar panels were 2 layers of magnetic torque coils, which were in series. Each coil consisted of 50 wraps making a total of 100 wraps per axis.

A solar panel does not exist for H2's z-axis, so the z-axis magnetic torque coil was made from wrapping 30-gauge magnet wire into a coil around a round form with a total of 150 wraps and then encasing the coil with Kapton® tape (Fig. 28). The diameter of the form is such that when formed into a rectangle, the dimensions are large enough to fit around the CSI stack of H2, but small enough to allow the structure to enclose the coil and PCB stack (Fig. 29).

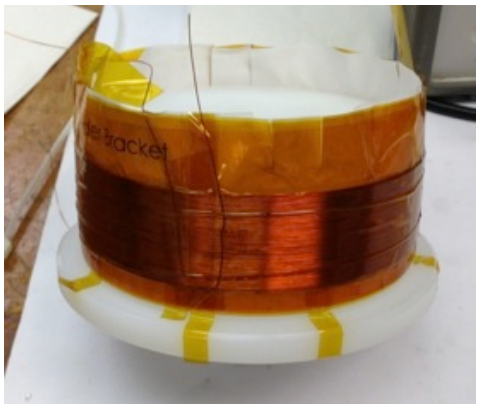

Figure 28: The z-axis magnetic torque coil wound on a form.

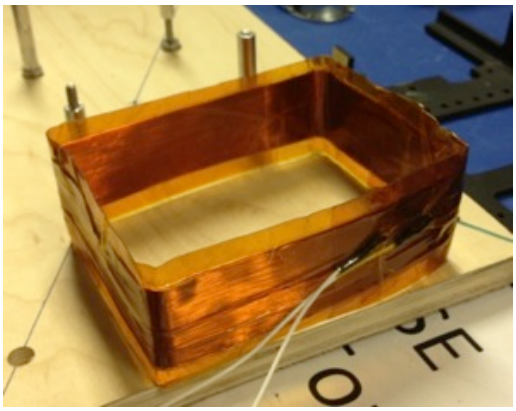

Figure 29: The formed z-axis magnetic torque coil formed into a rectangle.

3.1.4 Determination

Sensors for attitude determination consist of a set of nine photodiodes, a three-axis magnetometer, and a pair of infrared sensors. For the x and y axes in both directions and +Z axis there is only one photodiode mounted to the face; however, for the –Z axis there are a pair of photodiodes to prevent inaccurate readings due to shadowing on a single photodiode from the structure above it. Each photodiode is connected to a transimpedance amplifier that converts the short circuit current from each photodiode to a voltage that is proportional to the amplifier gain. This voltage is then read by an ADC on the ADCS board on the –Z face where, when using the maximum-current algorithm, the Sun vector in the body frame of H2 is estimated (Table 4). The short circuit current from a photodiode is proportional to the power received by the photodiode by the Sun. Since it is assumed that when H2 is in the Sun that the power from the Sun is constant, the change in power received by a photodiode is only due to a change in area of the projection along the Sun vector. The photodiode chosen for H2 was

the S25VR manufactured by OSI Optoelectronics [19]. The magnetometer used is the HMC5883L manufactured by Honeywell and is located on the nadir board mounted to the –Z face of H2 (Fig. 30) [10].

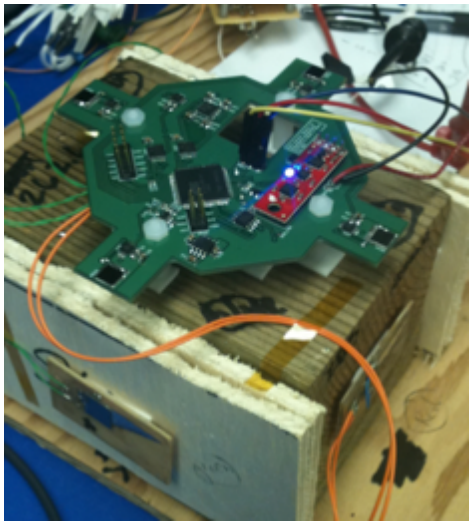

Figure 30: The nadir board test bed.

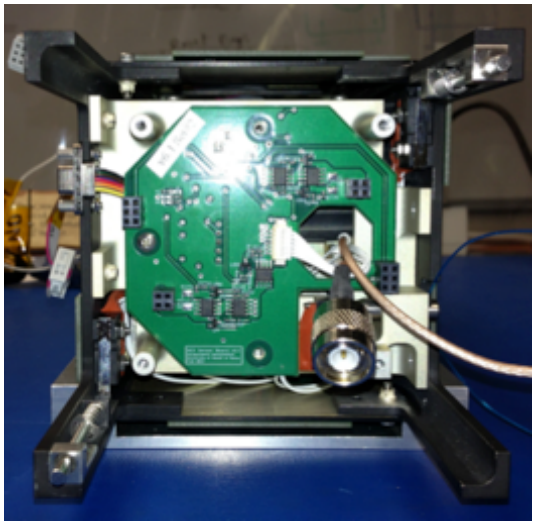

Figure 31: H2's ADCS board.

Table 4: The maximum current algorithm.

Read $i_x, i_{-x}, i_y, i_{-y}, i_z, i_{-z1}, i_{-z2}$

If $\{i_x, i_{-x}, i_y, i_{-y}, i_z, i_{-z1}, i_{-z2}\} > i_{min}$

if $i_{-z1} > i_{-z2}$ then $i_{-z} = i_{-z1}$

otherwise $i_{-z} = i_{-z2}$

if $i_z > i_{-z}$, then $i_z = i_z$

otherwise $i_z = -i_{-z}$

if $i_y > i_{-y}$ then $i_y = i_y$

otherwise $i_y = -i_{-y}$

if $i_x > i_{-x}$ then $i_x = i_x$

otherwise $i_x = -i_{-x}$

$$\mathbf{v}_S^B = \frac{[i_x\ i_y\ i_z]^T}{\sqrt{{i_x}^2 + {i_y}^2 + {i_z}^2}}$$

otherwise

$$\mathbf{v}_S^B = [0\ 0\ 0]^T$$

Chapter 4
Simulation Results

4.1 NADDS Initial Conditions

The initial conditions set in NADDS when entering the detumbing mode is that H2 has a rotation rate of 10 deg/sec/axis and has an identity attitude matrix relative to the ECI frame. This selection for the attitude matrix means that H2's body frame is aligned with the ECI frame at the start of the simulation, but has little effect on the final outcome of the simulation . The integrator used for the ODEs in (8) & (20) is the Rugga-Kutta method. Simultaneously, H2's attitude, represented by the quaternion, and body angular velocities are calculated. The quaternion vector is then converted to the attitude matrix using (6). As far as the integrator is concerned, it does not know of the different modes of H2 and only knows of the control and disturbance magnitudes and directions therefore only one set of initial conditions are required. Another way to view this is that the final state for the attitude and body angular velocities in a previous mode becomes the initial condition for the following mode.

4.2 Detumbling Time & Energy

The initial condition of 10 deg/sec/axis when entering detumble mode represents an unusually high tumbling rate and is not normally observed by other CubeSats launched by other universities. This high tumbling rate was selected to produce conservative energy estimates. At the beginning of the detumbling mode, soon after orbit insertion, the communications antenna is deployed. After this, there is no moment of inertia change until the stabilization mode. The rotation rate of the magnetic field vector near the equator for a nonpolar orbit is approximately $\frac{2\pi}{90\ min} = 0.0667\ deg/s$. This corresponds to the inertial rotation rate that the satellite would experience if it followed the magnetic field perfectly around the region of the equator when the magnetic field is approximately tangent to the Earth's surface. Therefore, this was set as the threshold to determine when the

satellite is sufficiently detumbled. Since the satellite is rotating on all three of its axes, the magnitude of the angular velocity is used to represent the satellite's tumbling state in a single number. The reasoning is that if the magnitude of the angular velocity is less than the cutoff velocity, then any given axis must have a tumbling rate less than or equal to the magnitude.

The detumbling time and energy requirement depends on if the B-Dot law is following the proportional approach, (31), or the bang-bang approach, (33). It is known that the rate of decay of the angular velocity for the bang-bang approach will always be greater than its proportional control law counterpart; however, the detumbling time for each case must be calculated numerically (Fig. 32).

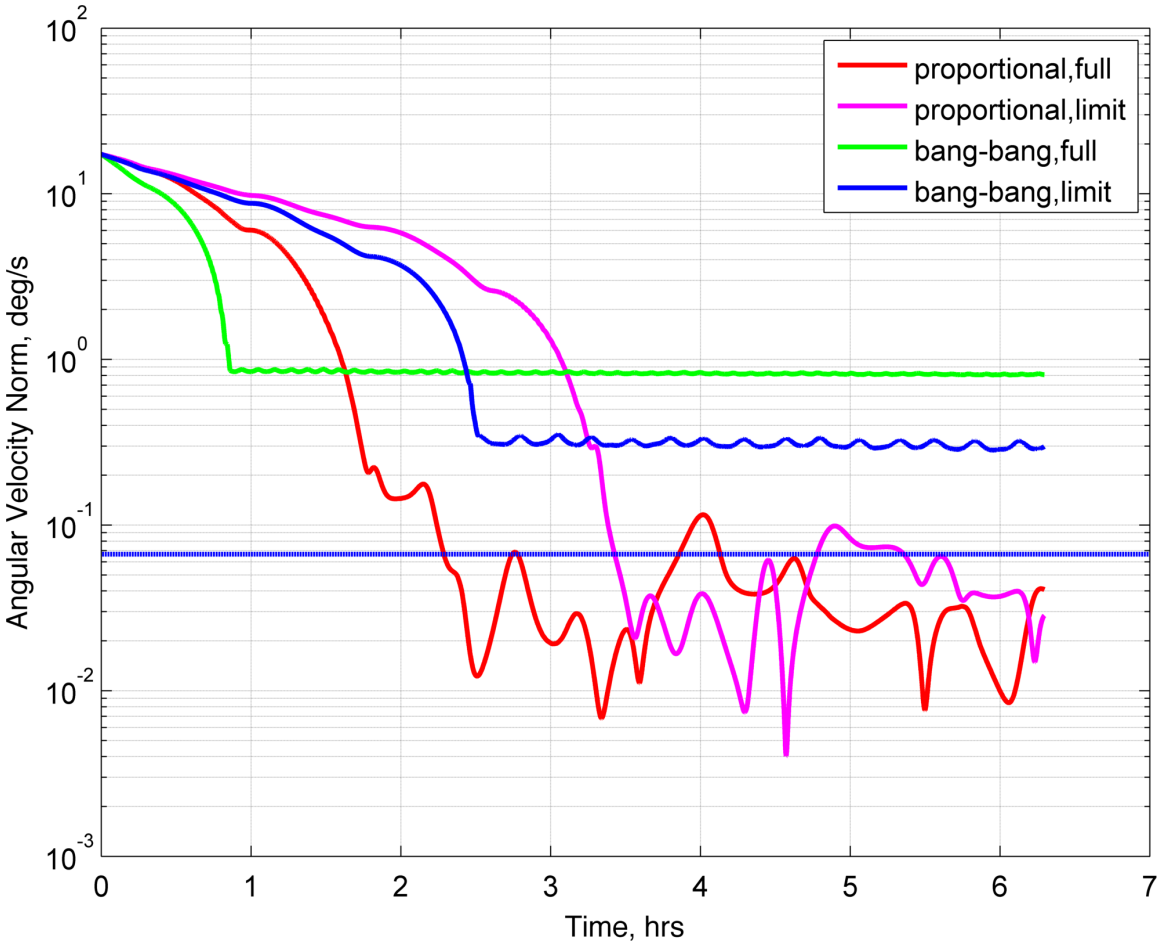

Figure 32: H2's simulated angular velocity for the proportional and bang-bang B-Dot control laws. The flat blue line represents the approximate angular velocity of a satellite following the magnetic field over the equator.

Only the proportional control laws sufficiently detumble H2 to fall below the average angular velocity of the magnetic field.

Two cases were simulated for each of the proportional and bang-bang cases: full actuation and limited actuation. The full actuation case for both the proportional and bang-bang versions of the B-Dot control law use the full magnetic moment capability of each of the coils per axis whereas the limited actuation case limits the z-axis coil to have the same magnetic moment as either of the x and y axes. The dashed blue line spanning figure 32 represents the angular velocity corresponding to the rotation rate of a magnetic field vector when the satellite is close to the equator.

4.2.1 Detumbling Time

Of all detumble control law formulations, the proportional B-Dot control law with full control authority was the only version that met the requirement to completely detumble the satellite to less than $0.0667\ \mathrm{deg/sec}$ while requiring the lowest amount of time at just under 1.45 orbits (2.29 hours). The second combination that fully detumbled the satellite was the proportional B-Dot control law with the limited control authority and had a longer detumbling time just under 2.18 orbits (3.43 hours). Neither the fully or limited actuation cases of the bang-bang control laws fully detumbled the satellite. Like the theory predicted, the full actuation, bang-bang law dissipated H2's rotational kinetic energy faster rate than the full actuation, proportional law [17]. However, it did not fully detumble the satellite to less than $0.0667\ \mathrm{deg/sec}$ and settled at about 0.8 deg/sec. The bang-bang control law with limited control authority was more successful in detumbling H2, but still did not meet the goal and took much longer to reach its steady value of 0.3 deg/sec.

4.2.2 Detumbling Energy

Another factor in choosing which of the detumbling laws to use was the energy consumption of each law (Fig. 33).

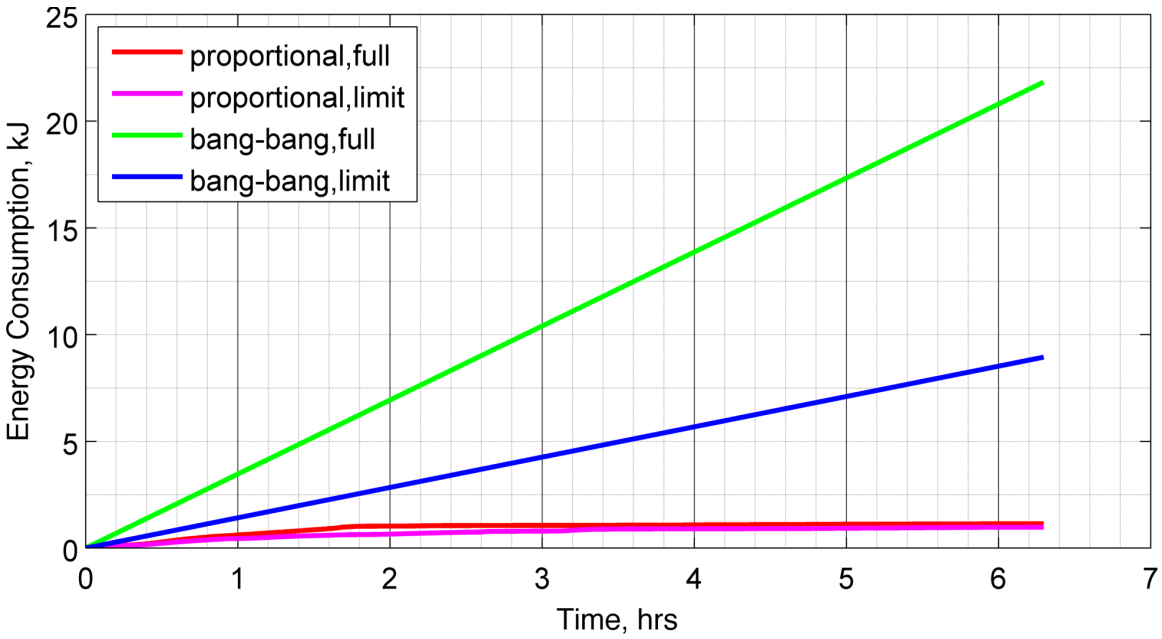

Figure 33: The energy consumption for the bang-bang and proportional detumbling schemes. The bang-bang detumbling schemes are much more power hungry than the proportional schemes. The bang-bang schemes consume power in a linear fashion as opposed to the proportional schemes which taper off gradually as the tumbling velocity decreases.

Considering just the joule-heating losses within the coils, the energy required to detumble via the proportional full control authority B-Dot law is 1.052 kJ. This is the law that requires the least time to fully detumble H2. To estimate the energy for the bang-bang control laws is difficult as the angular velocity of H2 does not completely fall to our target rate of 0.0667 deg/s. However, since we see that the angular velocity settles to a steady state value after some time for each case, the best estimate we can make for the energy consumption for these cases is to use the time when the satellite begins tumbling at this steady velocity as the time that the detumbling law finishes. Table 5 summarizes the various energy consumptions and times for the different detumbling laws.

Table 5: Simulation results for detumbling mode energy and time.

Method		Energy Consumption (kJ)[Wh]	Time (orbits)[hours]
Proportional	Full actuation	1.052 [0.292]	1.453 [2.287]
	Limited actuation	0.890 [0.247]	2.177 [3.427]
Bang-Bang	Full actuation	2.985 [0.829]	0.547 [0.861]
	Limited actuation	3.591 [0.998]	1.605 [2.527]

4.3 Alignment Time

At the beginning of the alignment mode, H2 is essentially at a standstill with respect to the ECI frame, but H2 can be pointed in any direction since the detumble controller only dissipates H2's rotational kinetic energy and does not give preference to a final attitude for H2. To make H2's orientation deterministic, the alignment mode is activated to align H2 with the Earth's magnetic field. During this mode there are no changes in H2's inertia. Since the alignment mode uses a control law that is very similar to the detumbling law, the proportional B-Dot law with full control authority was used.

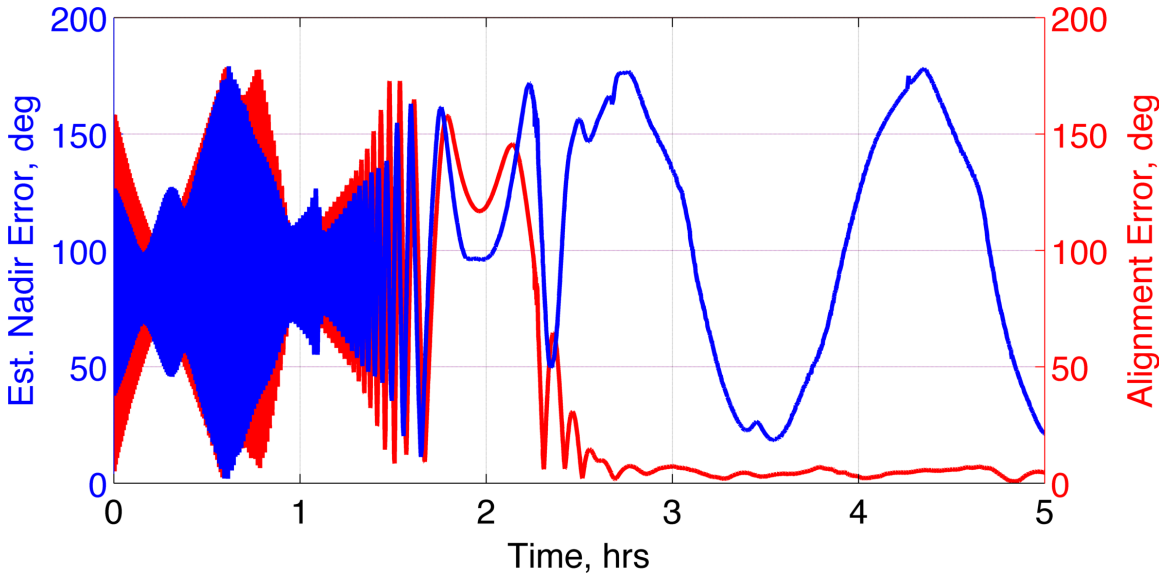

Figure 34: The alignment error and estimated nadir error. The alignment error stabilizes to zero when alignment mode is activated and the nadir error becomes periodic since H2 is locked onto the magnetic field.

Two conditions are required to conclude the alignment mode – the nadir error must be less than 90 degrees and the alignment error must be close to zero. A nadir error less than 90 degrees will ensure that H2 will stabilize so that the transponder antenna points in the nadir direction and an alignment error close to zero shows that H2 is indeed tracking Earth's magnetic field. Ideally, the moment that these two conditions are met, stabilization mode can be initiated and the gravity-gradient boom can be deployed. However, since a command must be sent from the ground, it is unlikely that this will be the case since H2 will pass over Hawai‘i only three times a day. Instead, H2 will likely be "parked" to the magnetic field for up to eight orbits before the earliest opportunity arises to give the "okay" from the ground station to deploy the boom (Fig. 34). For the sake of this paper, let's assume a best and worst case alignment time. The best case would be as soon as both conditions are met. The worst case will be after a half-day when H2 is assumed to have just passed over Hawai‘i and then when both conditions are met afterwards. Since H2 can essentially choose when to deploy the boom after the okay is given, the best time to deploy the boom is when the nadir error is at its lowest. This will produce the lowest time required to dissipate oscillations due to the increase in the gravity-gradient torque.

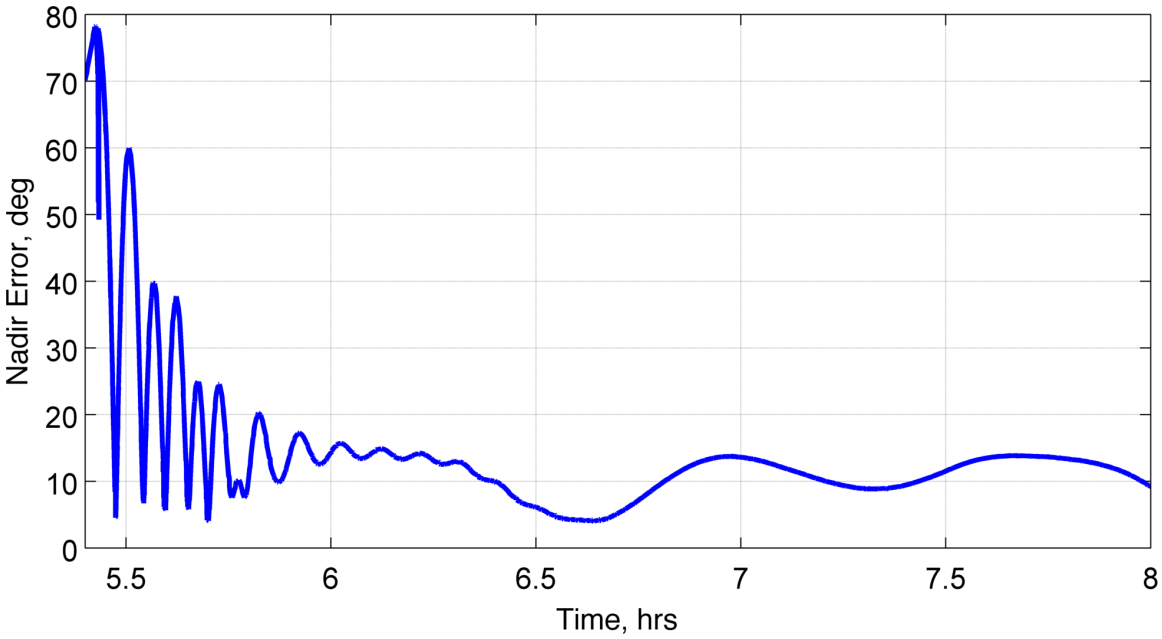

Figure 35: The nadir error after the gravity gradient boom and the stabilization mode is activated. Including air drag, the nadir pointing error falls to less than 14 degrees within one orbit from deploying the boom

4.4 Stabilization Time

Assuming that a command has been given to deploy the boom and the gravity-gradient capture conditions are met, the stabilization mode begins with the extension of the gravity-gradient boom. Gravity-gradient capture implies that H2 has been tracking Earth's magnetic field, has lost most of its rotational kinetic energy and H2's $-\mathrm{e}_3$ direction (the transponder antenna pointing direction) has a true nadir error of less than 90 degrees. The inertia increases on the x- and y-body axes by a factor of nearly 100 times after deployment. This increase takes the gravity-gradient torque from being a disturbance torque to a dominant control torque. However, deploying the boom also increases the aerodynamic disturbance torque on the boom. The gravity-gradient torque will align H2 with the closest lowest energy equilibra and assuming that the gravity-gradient capture conditions are met, this will correspond to H2 pointing with its transponder antenna pointing in the nadir direction.

After deployment of the boom, it only takes approximately 1 orbit (~90 min) to achieve gravity-gradient capture and the nadir error falls below 15 degrees (Fig. 35). Since the nadir error is close to zero, as opposed to 180 degrees, this indicates that the –z body axis is pointing in the nadir direction.

4.5 Attitude Determination Error

During the alignment mode, the nadir error estimate is the figure of merit that is telemetered to the ground station to determine if H2 is ready to deploy its gravity-gradient boom. Two conditions must be met to issue the gravity-gradient boom command: the true nadir error must be less than 90 degrees and H2 must be tracking the magnetic field. The confidence in the nadir pointing error estimate is important since once the boom deployment command is sent, there is no way to stop the deployment. If the estimate error is too great and H2 had an estimated nadir pointing error bordering 90 degrees, deploying the boom can be catastrophic towards achieving the nadir orientation. Therefore the estimate error must be characterized. Below, the nadir error estimate error is calculated for the entire simulation (Fig. 36). There are several sources that contribute to the error in the nadir error estimate. These include, noise in the current measurements of the photodiodes, noise in the magnetometer readings, and errors in the interpolation of the magnetic field. Since the attitude estimation scheme is nonlinear it is difficult to quantify how each source independently affects the total error. However, the absolute error in the nadir error estimate can is calculated by taking the absolute value of the difference between the true nadir error calculated by the orbit model and the nadir error which is calculated by (19) and using the TRIAD estimation scheme.

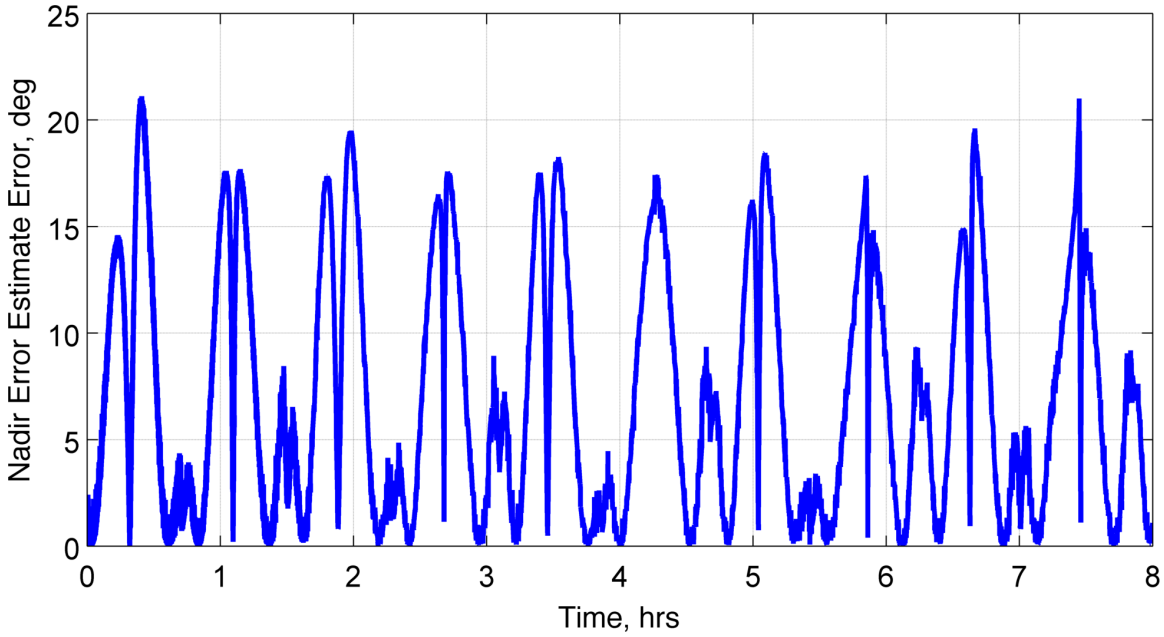

Figure 36: The error in the estimated nadir error. The error in the nadir error estimate is bounded to less than 22 degrees.

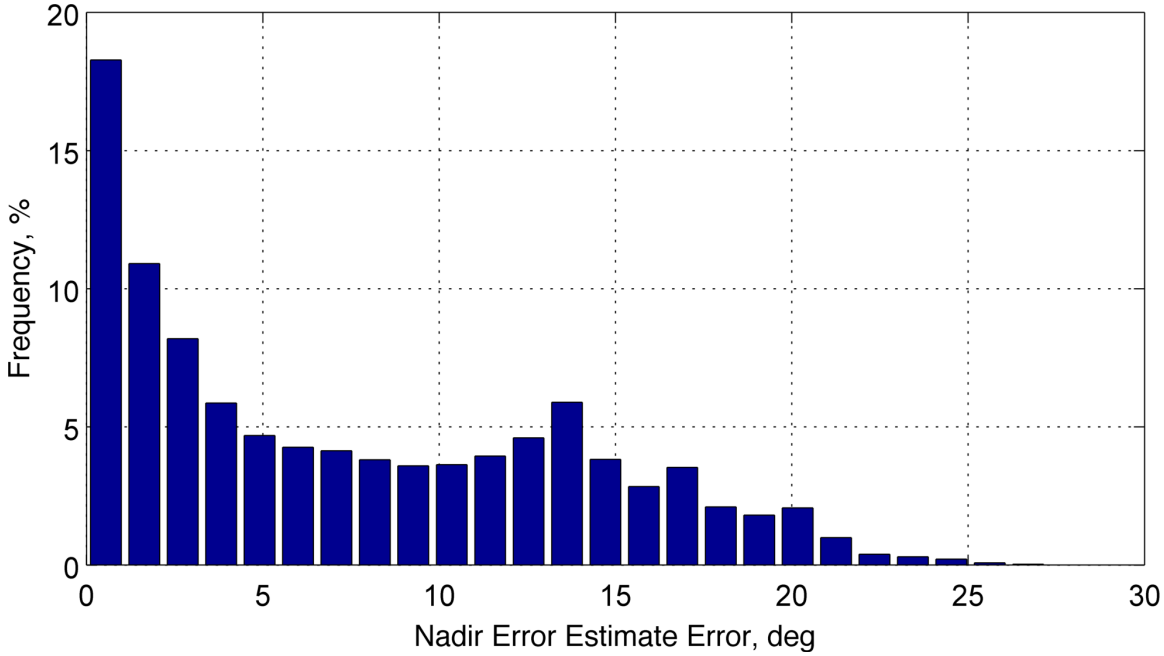

Figure 37: The frequency of the error in the nadir error estimate. Majority of the error in the nadir error estimate is less than 10 degrees.

The nadir error estimate error appears to be bounded within 22 degrees. Also, the error does not seem to depend much on the orientation of H2 relative to the Sun or magnetic fields; if this were the case, we would see much more activity

during the first orbit when the detumbling mode is activated. Taking a closer look at the behavior of the nadir error estimate error, we create a histogram of the error (Fig. 37). The histogram totals the occurrences of a particular error and creates a plot of these totals. By dividing the totals by the number of data points in Figure 36, a histogram showing the frequencies of occurrence of the errors are calculated.

Here, we clearly see that all the errors are bounded to be less than 22 degrees. Furthermore, majority of the errors are less than 10 degrees. We want to have a confidence metric that lets us know how likely a given error is present in the estimate (Fig. 38).

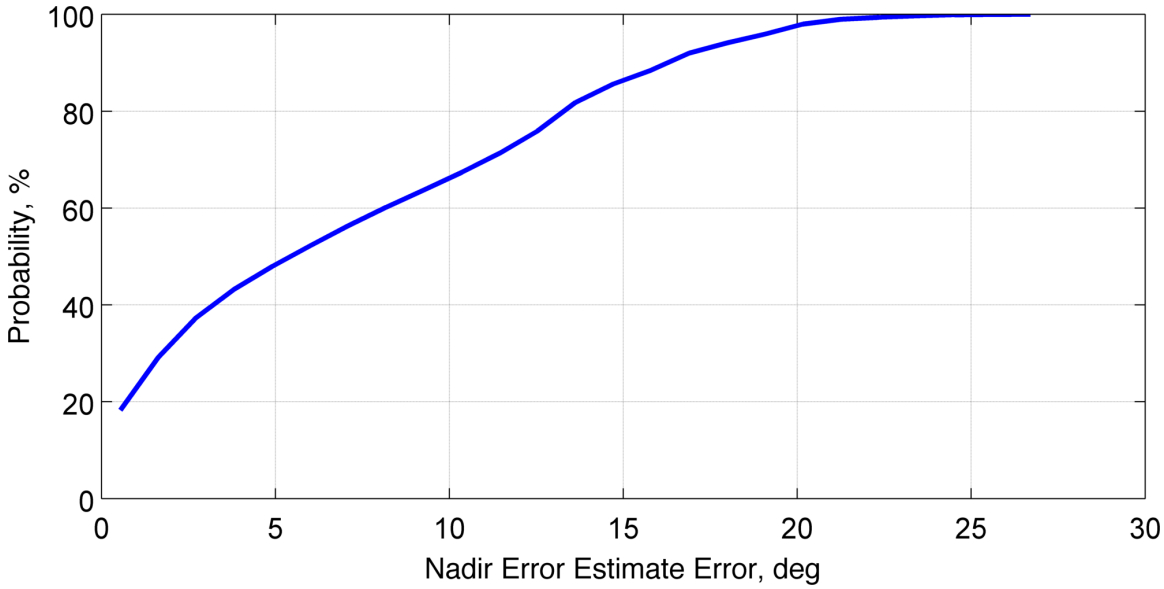

Figure 38: The probability of error in the nadir error estimate. The error in the nadir error estimate is almost guaranteed to be within 20 degrees.

One can conclude that there is a 100% probability that the error in a given nadir error estimate is less than 22 degrees. On the other hand, there would be a 65% probability that the error is less than 10 degrees. This means that to be safe, H2 should not be commanded to deploy the boom until the nadir error estimate reads 68 degrees or less. This will ensure that H2 will stabilize to point the transponder antenna in the nadir direction regardless of the error.

4.6 Alignment & Stabilization Mode Energy Consumption

Of all the modes, the alignment mode consumes the most energy from the battery (Fig. 39). This is consistent with predictions since the z-axis magnetic torque coil is energized at half its capacity for the entire time of the alignment mode.

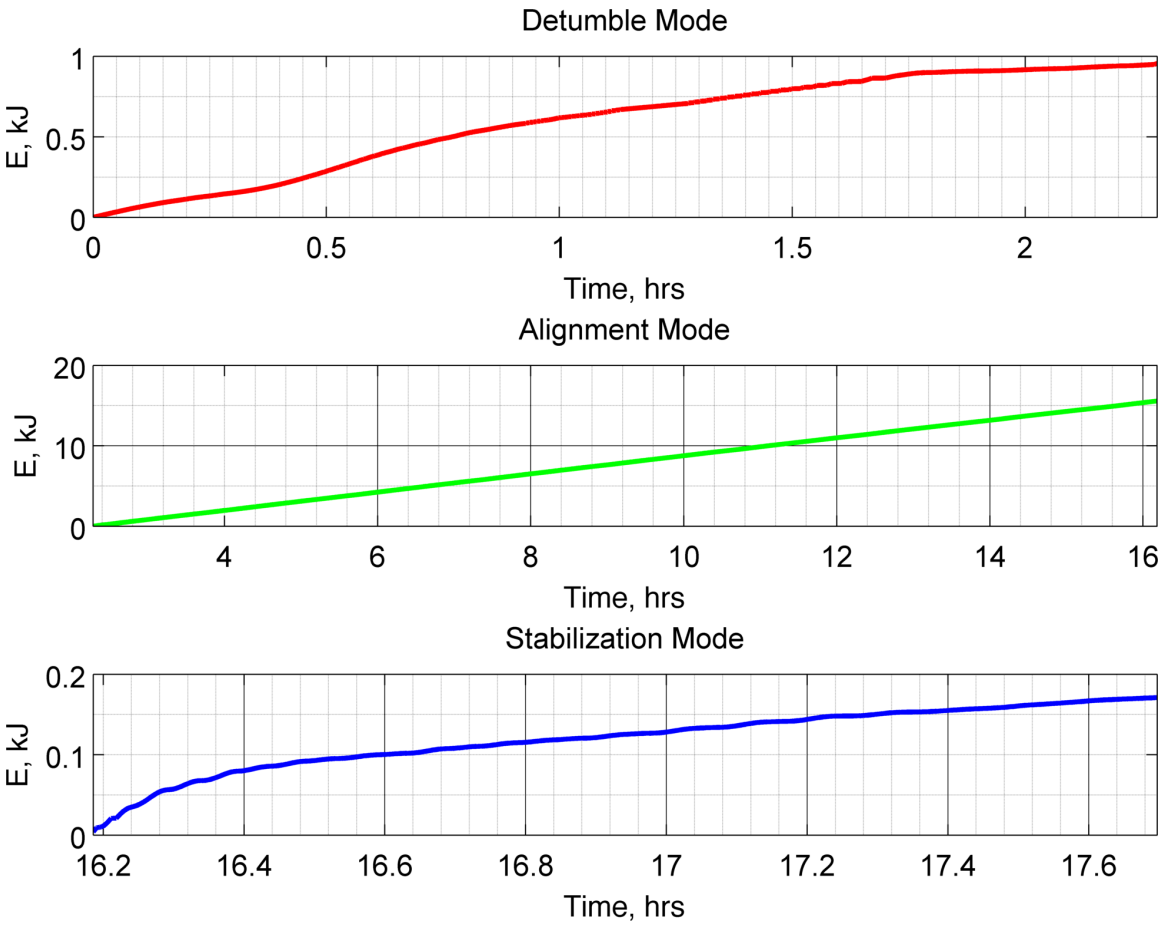

Figure 39: The energy consumption for the detumble, alignment, and stabilization modes. The energy consumption for the detumbling mode tapers off with time while the alignment mode energy consumption rate remains constant and is the largest of all three modes. Relatively little energy is consumed during stabilization.

If the deploy boom command is sent while H2 is passing over Hawai‘i at the same moment H2 locks onto the magnetic field and the nadir pointing error is

less than 90 degrees, the minimum energy required for the alignment mode can be as low as 0.467 kJ. It would likely require another half orbit or so to successfully stabilize to the nadir position and detumbling would take 1.05 kJ. The total minimum energy consumption for the ADCS mission would be about 2.38 kJ or 0.66 Wh.

It is not likely for the first pass over Hawai‘i to be so soon and can be as long as 12 hours after orbit insertion. Since the alignment mode consumes the most energy, H2 remaining parked in the Earth’s magnetic field for half a day can consume a considerable amount of energy. If the deploy boom command is sent exactly after 12 hours after orbit insertion, the boom would take approximately another half orbit or so until H2 will be in a position to deploy the boom. After deploying the boom, it would take another orbit or two to stabilize in the nadir position. In this scenario, the energy consumption for the ADCS mission would be about 13.11 kJ or 3.64 Wh.

If the command is not sent on this pass, each successive opportunity will occur an additional 7.7 orbits or 12.12 hours later. With H2 held in the alignment mode during this time, an additional 1.73 kJ/orbit or 0.48 Wh/orbit would be consumed. Amounting to 13.19 kJ/half-day or 3.66 Wh/half-day.

4.7 Battery Energy Consumption Estimate Summary

The onboard battery has a capacity of approximately 346 kJ (96 Wh). If H2 is held in alignment mode for the half-day it would consume approximately 4% of the battery’s capacity. Therefore for each uplink opportunity, approximately 4% would be consumed by ADCS alone. With the lithium radio consuming approximately 0.2 W in receive mode during all ADCS modes, an additional 8.73 kJ or 2.42 Wh, or 2.5% of charge capacity would be consumed between uplink opportunities. For every half-day, approximately 6.5% would be consumed while H2 is in the alignment mode awaiting the deploy boom command. At a 50% Depth of Discharge (DoD) cutoff, this would mean that H2 could stay in alignment

mode for up to 3.8 days before being forced into charge mode. This would give between seven and eleven opportunities after launch to send the command to deploy the boom before H2 would be forced into charging mode and in turn disable alignment mode. Assuming that the solar panels have a Maximum Power Point Tracking (MPPT) capability, a solar cell efficiency of 28%, and zero power draw during charge mode, each orbit could generate up to 18 kJ of energy. With a depth of discharge of 50%, a total of 15 hours would be required to return the battery to a full charge.

4.8 Results Summary

The minimum and maximum times and energies required by each mode of H2's ADCS mission is summarized in Table 6. Key impositions that H2's ADCS has on the mission and satellite on a system level is summarized in Table 7.

Table 6: The ADCS mission time and energy consumption estimates.

Mode	Min. Time (hrs) [Orbits]	Max Time (hrs) [Orbits]	Min. Energy (kJ) [Wh]	Max. Energy (kJ) [Wh]	Max. Error (deg)
Detumbling	2.29 [1.45]	2.29 [1.45]	1.05 [0.29]	1.05 [0.29]	--
Alignment	0.91 [0.58]	10.42 [6.62]	1.086 [0.30]	11.81 [3.28]	8.0
GG Stabilization	1.21 [0.76]	1.69 [1.07]	0.20 [0.06]	0.25 [0.07]	14.0
TOTAL	4.41 [2.80]	14.4 [9.15]	2.34 [0.65]	13.11 [3.64]	--

Table 7: Time and energy key findings from NADDS.

Minimum ADCS mission energy consumption	2.34 kJ [0.65 Wh]
Nominal ADCS mission energy consumption	13.11 kJ [3.64 Wh]
Alignment mode energy consumption per half day	13.2 kJ [3.67 Wh]
Alignment mode DoD per half day	4%
Alignment mode + Lithium 1 DoD per half day	6.5%
Max days for alignment mode	3.8 days
Total uplink opportunities (single charge)	7-11

Chapter 5
Conclusion

The University of Hawai‘i’s first 3U CubeSat, H2, was developed at the UH Small-Satellite Laboratory. Its mission is to aid in the calibration process of Air Force radar stations in the United States. A directional antenna on H2 imposes a requirement that the satellite must point in the nadir direction. An ADCS was designed to meet this requirement and the NADDS was developed to analyze its performance. The inner workings of the NADDS is outlined through the use of mathematics where the gravity-gradient and magnetic moment control torques and the aerodynamic disturbance torque on H2 was defined.

To achieve nadir stabilization, the task was split into three modes: detumbling, alignment and gravity-gradient stabilization. Each of these modes was simulated, and the time and energy required by each mode was determined.

Two detumbling laws were proposed: the proportional and bang-bang B-Dot detumbling laws. It was shown that the proportional detumble control law with full actuation produced the lowest detumbling time and required the least energy. Although the bang-bang approach may be favored due to its simplicity, and as theory predicted, did dissipate the satellite’s kinetic energy at a much faster rate than the proportional controller, it ultimately did not meet the detumbling rotational velocity requirement. Therefore, the proportional detumbling controller with full actuation was chosen for implementation.

The alignment mode’s pointing time, error, and energy consumption was estimated. As H2 does not pass over Hawai‘i every orbit, the energy required by alignment mode is greatly dependent on when the command is given to deploy the boom. Since this command can only occur when H2 passes over Hawai‘i, the time that H2 might be in alignment mode tracking the magnetic field is at least 12 hours and possibly longer depending on the readiness of the ground station to

validate the nadir error estimate based on telemetered data. The error in the nadir error estimate was analyzed and a bound on the error was found based on an empirically-calculated confidence probability.

Lastly, the stabilization mode was simulated and based on when H2 is given the command to deploy the boom, the time and energy required were estimated. The NADDS was proven to be an invaluable tool to evaluate the expected performance of H2's ADCS.

5.1 Future Work

The development of the NADDS represents a large accomplishment; however, it lacks several key features that would be valuable in an attitude simulator.

First, it would be useful to model the gravity-gradient boom deployment disturbance torque. Within this work, it was assumed that the boom reel gathers speed for only a fraction of a second before stabilizing to 60 deg/sec, thus the disturbance torque was assumed to be short-lived and cause negligible effect on the nadir error. The validity of this assumption needs to be evaluated.

Secondly, it is well known that the Runge-Kutta integrator used for attitude propagation is ill-suited for simulating satellite dynamics for long durations. Since the simulation times are on the order of a day or two, and tolerances of the integrator were set sufficiently small to ensure numerical dissipation is small, yet large enough to ensure relatively short simulation times, this is a sufficient solver for the purposes of this paper. However, since the rotation of a satellite evolves on a nonlinear space, the Runge-Kutta is ill-suited as it is designed for a linear space. A better-suited integrator would be a Lie Group Variational Integrator (LGVI), which preserves the orthonormal constraint on the rotational matrix and preserves energy for long simulation times such as for weeks at a time. Such an integrator would be essential for simulating magnetic hysteresis rod dynamics since their retarding torque is very small and would require weeks of simulation

time. A Runge-Kutta method would require such a small tolerance in error to simulate the hysteresis effect such that simulating for weeks would be computationally time prohibitive.

Last, the simulation programs structure could be cleaned up by compartmentalization using Simulink® and a GUI would increase user-friendliness.

References

[1] D. Castelvecchi. (2014, Jan. 30) *Affordable Orbital: Tiny Satellites Make for Democratic Access to Space*. [Online]. Available: http://www.scientificamerican.com/article/cubesats-photos/

[2] G. D. Krebs. (2013, Nov. 25). *RadCal (P92-1)*. [Online]. Available: http://space.skyrocket.de/doc_sdat/radcal.htm

[3] T. Lawrence. (2013, Dec. 13). *Satellite's operation time exceeds expectations*. [Online]. Available: http://www.kirtland.af.mil/news/story.asp?id=123357111

[4] Z. Tudor, “Design and Implementation of Attitude Control for 3-axes Magnetic Coil Stabilization of a Spacecraft,” M.S. thesis, Norwegian Univ. of Sci. and Tech., Norway, 2011.

[5] B. Wie, *Space Vehicle Dynamics and Control*. Reston, Virginia: American Institute of Aeronautincs and Astronautics, 2008..

[6] J. L. Junkins and J. L. Crassidis, *Optimal Estimation of Dynamic Systems*. Boca Raton, FL: Chapman & Hall/CRC Press, 2004.

[7] J. Meeus, *Astronomical Algorithms*.Richmond, VA: Willmann-Bell, 1998.

[8] M. J. Sidi, *Spacecraft Dynamics & Control*. New York, NY: Cambridge Univ. Press, 1997.

[9] D. A. Vallado, *Fundamentals of Astrodynamics and Applications*. Hawthrone, CA,: Microcosm Press, 2007.

[10] *3-Axis Digital Compass IC HMC5883L*, Honeywell International Inc., Plymouth, MN, 2013.

[11] K. L. Makovec, “A Nonlinear Magnetic Control for Three-Axis Stability of Nanosatellites,” M.S. thesis, Virginia Polytechnic Inst. and State Univ., Blacksburg, VA, 2001.

[12] J. Davis, “Mathematical Modeling of Earth's Magnetic Field,” Virginia Inst. of

Tech., Blacksburg, VA, Tech. Note. 2004.

[13] C. Roithmayr, “Magnetic Field Model,” Spacecraft and Sensors Branch (CBC), NASA Langley Research Center, Greenbelt, Model Code 1998.

[14] J. A. Bowen, “On-Board Orbit Determination and 3-Axis Attitude Determination for Picosatellite Applications,” M.S. thesis, California Polytechnic State Univ., San Luis Obispo, CA, 2009.

[15] H. D. Black, “A passive system for determining the attitude of a satellite,” *AIAA Journal*., vol. 2, pp. 1350-1351, 1964.

[16] R. E. Fischell and F. F. Mobley, “A System for Passive Gravity-Gradient Stabilization,” in *AIAA Guidance and Control Conf.*, New York, NY, 1963.

[17] T. W. Flatley *et al.*, “A B-Dot Acquisition Controller for the RADARSAT Spacecraft,” Code 712/Guidance, Navigation and Control Branch, Goddard Space Flight Center, Greenbelt, 1997.

[18] K. Svartveit, “Attitude Determination of the NCUBE Satellite,” M.S. thesis, Norwegian Univ. of Sci. and Tech., Norway, 2003.

[19] *Solderable Chip Series*, OSI Systems, Inc., Hawthorne, CA, 2013.

[20] *Permanent Magnet Brake Type 14.120.XX.103*, Kendrion Magneta, Aerzen, Germany, 2014.